Detection of K⁺ Efflux from Stimulated Cortical Neurons by an Aptamer-Modified Silicon Nanowire Field-Effect Transistor

Ankur Anand,[†,‡,§] Chia-Rung Liu,[§,⊥] Ai-Chuan Chou,[‖] Wan-Hsuan Hsu,[‖]
Rajesh Kumar Ulaganathan,[†,§,⊥] Yi-Cheng Lin,[#] Chi-An Dai,[#] Fan-Gang Tseng,[‡] Chien-Yuan Pan,*[‖]
and Yit-Tsong Chen*[§,⊥]

[†]Nanoscience and Technology Program, Taiwan International Graduate Program, Academia Sinica, Taipei 115, Taiwan

[‡]Department of Engineering and System Science, National Tsing Hua University, Hsinchu 30013, Taiwan
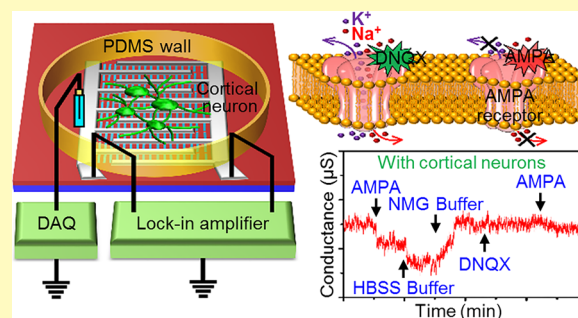
[§]Institute of Atomic and Molecular Sciences, Academia Sinica, Taipei 106, Taiwan

[‖]Department of Life Science, [⊥]Department of Chemistry, and [#]Department of Chemical Engineering, National Taiwan University, Taipei 106, Taiwan

Ⓢ *Supporting Information*

ABSTRACT: The concentration gradient of K⁺ across the cell membrane of a neuron determines its resting potential and cell excitability. During neurotransmission, the efflux of K⁺ from the cell via various channels will not only decrease the intracellular K⁺ content but also elevate the extracellular K⁺ concentration. However, it is not clear to what extent this change could be. In this study, we developed a multiple-parallel-connected silicon nanowire field-effect transistor (SiNW-FET) modified with K⁺-specific DNA-aptamers (aptamer/SiNW-FET) for the real-time detection of the K⁺ efflux from cultured cortical neurons. The aptamer/SiNW-FET showed an association constant of $(2.18 \pm 0.44) \times 10^6$ M⁻¹ against K⁺ and an either less or negligible response to other alkali metal ions. The α-amino-3-hydroxy-5-methyl-4-isoxazolepropionic acid (AMPA) stimulation induced an outward current and hyperpolarized the membrane potential in a whole-cell patched neuron under a Na⁺/K⁺-free buffer. When neurons were placed atop the aptamer/SiNW-FET in a Na⁺/K⁺-free buffer, AMPA (13 μM) stimulation elevated the extracellular K⁺ concentration to ~800 nM, which is greatly reduced by 6,7-dinitroquinoxaline-2,3-dione, an AMPA receptor antagonist. The EC₅₀ of AMPA in elevating the extracellular K⁺ concentration was 10.3 μM. By stimulating the neurons with AMPA under a normal physiological buffer, the K⁺ concentration in the isolated cytosolic fraction was decreased by 75%. These experiments demonstrate that the aptamer/SiNW-FET is sensitive for detecting cations and the K⁺ concentrations inside and outside the neurons could be greatly changed to modulate the neuron excitability.

KEYWORDS: aptamer, biosensor, ion channel, neuron, potassium ion, silicon nanowire field-effect transistor

The asymmetric distribution of ions across a cell membrane is important for various cellular activities, such as body fluid electrolyte balance,[1] acid−base balance,[2] apoptosis,[3] neurotransmission,[4] and muscle contraction.[5] The potassium ion (K⁺) is the predominant cation inside a cell at the concentration (C_{K^+}) level of ~140 mM. In contrast, the extracellular K⁺ concentration ($C_{K^+}^{ex}$) is typically ~5 mM. Comparatively, Na⁺ has the opposite asymmetric concentration (C_{Na^+}) distribution pattern to what K⁺ has. In the nervous system, the resultant ionic gradients of Na⁺ and K⁺ across the cell membrane are crucial to the generation of neuronal electrical signals, including the resting membrane potential, the action potential, and the synaptic potentials.[6] Because extracellular K⁺ ions diffuse in the very limited volume in the interfacing space among neurons, even a modest K⁺ efflux from neuronal cells can elicit considerable changes in $C_{K^+}^{ex}$.[7] An

elevation in the $C_{K^+}^{ex}$ will then affect the excitability of neurons, but the extent of the exact $C_{K^+}^{ex}$ changes remains unclear.

Advancements in nanotechnology over the past decade have resulted in the emergence of novel, sensitive nanoscale sensors. The high surface-to-volume ratio and the unique quantum mechanical properties of nanomaterials make them ideal candidates for the fabrication of biological/chemical sensors.[8−16] Moreover, due to their small sizes, nanomaterials can compatibly form an interface with biological entities, such as proteins, DNA, ribozymes, and so forth. Among the nanoscale sensors, silicon nanowire field-effect transistors (SiNW-FETs) have been extremely successful in sensing a variety of target molecules in real-time with label-free, sensitive,

and selective detections.[8−13,15−19] The binding of biomolecules on the SiNW surface leads to a significant conductance change inside the SiNW-FET due to an electrical gating effect. By modifying a suitable receptor on the SiNW surface, this SiNW-FET platform can be an excellent biosensor for detecting specific target biomolecules. While several technical improvements have been made in the past years to increase the detection sensitivity of SiNW-FETs, e.g., sensing in the subthreshold regime,[20] a frequency-domain measurement,[21] and selective surface modification,[22] efforts have also been directed to entrap numerous SiNWs between the source and drain electrodes, called a multiple-parallel-connected (MPC) SiNW-FET, where a cumulative response, resulting from multitudinous target-receptor bindings, could yield a drastic signal increase.[23]

The telomeres of human DNA consist of many d-(TTAGGG) repeats, which form a structure called the G-quadraplex and offer a unique K^+ binding site.[24,25] In recent years, many short single-strand oligonucleotides, 20−120 nucleotides, have been identified to possess specific binding abilities to various molecules. These oligonucleotides, called aptamers, are widely applied to biological research as sensors (aptasensors)[23] and therapeutic tools[26] to regulate cellular processes.[27] In this report, we modified K^+-specific DNA-aptamers on an MPC SiNW-FET (referred to as aptamer/SiNW-FET hereafter) to monitor the K^+ efflux from stimulated living neurons with a high detection sensitivity and target selectivity. Henceforth, we utilized this biosensor to probe and quantitate the $C_{K^+}^{ex}$ changes around live neurons. The use of aptamer/SiNW-FETs has several advantages compared with other binding affinity-based biosensors. First, the molecular size of an aptamer is generally smaller than conventional receptors (e.g., enzymes or antibodies), and therefore, the captured target molecules are drawn closer to the SiNW-FET surface, resulting in a stronger gating electrical field, yielding optimal detection signals. The closer distance from the target-receptor binding site to the SiNW-FET surface also minimizes the Debye−Hückel screening effect.[28] Second, in contrast to antibodies that have to be produced in vivo, aptamers can be synthesized using in vitro methods. This eliminates the need for laboratory animals in the antibody development and achieves minimal variability from batch-to-batch sensor production. Third, an aptamer formed by oligonucleotides is thermally stable compared with proteins and antibodies, which may lose their functionality irreversibly under thermal/chemical challenging environments. Furthermore, denatured aptamers can recover their functions by spontaneously refolding to return to their ambient status, which makes it possible to develop reusable aptamer/SiNW-FET biosensors. In the past, a cationic conjugated polymer-G-quadruplex assembly,[29] a G-quadruplex-induced aggregation of gold nanoparticles,[30] and an electrochemical aptasensor[31] were developed for the selective detection of K^+, but their applicability to biological systems is limited by the complicated nature of their sample matrix. In addition, a labeling process makes the experiments relatively complex, time-consuming, and expensive. Moreover, many of them require complicated instrumentation and involve cumbersome laboratory procedures, which restrict the scope of their practical application.
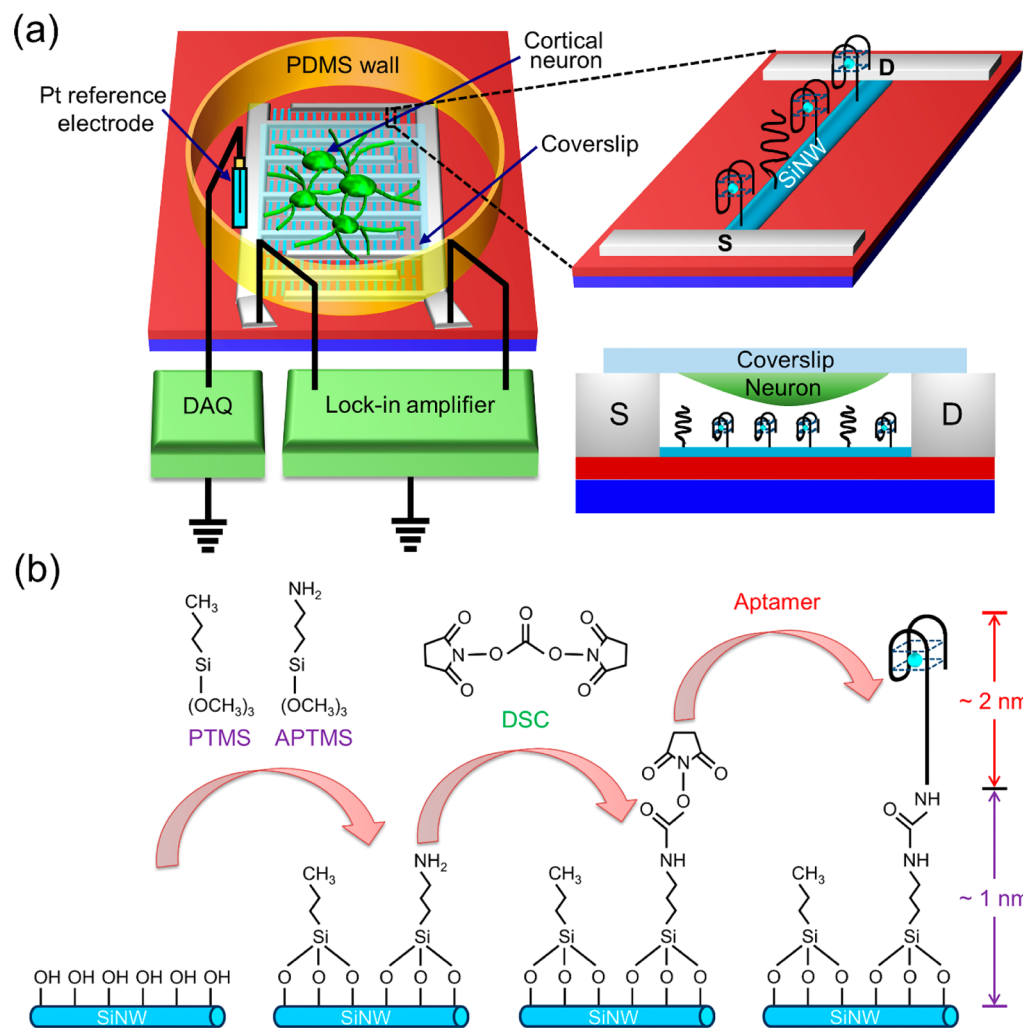
Several earlier studies of adopting micrometer-sized metal-oxide semiconductor FET (MOSFET) for the investigation of the K^+ ions released from living cells were reported; however, these employed MOSFET devices were not modified with a specific receptor to confer the target selectivity for K^+.[32−34] In this study, we utilized aptamer/SiNW-FETs to measure the $C_{K^+}^{ex}$ released from stimulated living cortical neurons. We examined the electrical responses of an aptamer/SiNW-FET to the escalated K^+ efflux from α-amino-3-hydroxy-5-methyl-4-isoxazolepropionic acid (AMPA)-stimulated neurons. With the neurons pretreated using 6,7-dinitroquinoxaline-2,3-dione (DNQX), an antagonist of AMPA, a substantial suppression of the AMPA-induced conductance change in the aptamer/SiNW-FET was detected. In addition, the C_{K^+} in the isolated cytosolic fraction detected by aptamer/SiNW-FET was decreased by ∼75% after AMPA stimulation. These electrical measurements with aptamer/SiNW-FETs allow us to quantitate the $C_{K^+}^{ex}$ released from stimulated living neurons and to characterize the C_{K^+} on both sides of the cell membrane. Henceforth, our novel approach provides a tool to study how the C_{K^+} fluctuation modulates the neurotransmission.

■ EXPERIMENTAL SECTION

Fabrication of the MPC SiNW-FET Devices. The MPC SiNW-FET devices were fabricated according to the procedures described previously.[23,35] Briefly, single-crystalline boron-doped SiNWs (Si:B = 4000:1) were grown catalytically with the assistance of 20 nm gold nanoparticles (Au NPs) in a chemical vapor deposition (CVD) reaction through the vapor−liquid−solid (VLS) growth mechanism. The Au NPs were dispersed onto a Si wafer chip with a 400 nm oxide layer, which had been incubated in a 0.1% aqueous solution of poly(L-lysine) for 10 min to increase the adhesion of the Au NPs. The Si wafer containing the Au NPs was then washed with deionized (DI) water, blown dry with N_2 gas, and cleaned in oxygen plasma (100 W and 50 sccm O_2 for 300 s). The p-type SiNWs were grown from the CVD reaction at 460 °C for 12.5 min in 10 sccm Ar, 6 sccm SiH_4 (10% in He), and 15 sccm B_2H_6 (100 ppm in He) at a total chamber pressure of 25 Torr. The diameters of the as-synthesized SiNWs were generally between 20 and 30 nm. The SiNWs were transferred onto a photoresist (S1805)-patterned Si wafer with a 400 nm oxide layer using a contact printing method. The SiNW-FET devices were fabricated following standard photolithographic procedures. The metal contact regions (defined by photolithography) were cleaned with oxygen plasma (100 sccm and 30 W). Meanwhile, the native silica sheath of the SiNW in the contact area was removed with a buffered oxide etching (BOE) solution. The metal layers (70 nm Ni and 100 nm Al) were deposited consecutively using thermal evaporation on the areas defined by a photomask with a few sets of interdigitated patterns. After liftoff, the MPC SiNW-FET devices were further annealed in forming gas (10% H_2 and 90% N_2) at 360 °C for 3 min to ensure a good electrical contact between the SiNWs and the metal electrodes. Meanwhile, the surface of the MPC SiNWs was thermally oxidized to form an insulating layer of silica to prevent both the charge transfer between the MPC SiNW-FET and the analyte molecules and an electrical leakage in the subsequent biosensing measurements in aqueous solution.

Immobilization of DNA-Aptamers on an MPC SiNW-FET. The as-fabricated MPC SiNW-FET chip was washed with ethanol and blown dry with N_2 gas. For surface modification, the MPC SiNW-FET chip was immersed in a 1% (v/v) ethanol solution of APTMS and PTMS (1:5) and allowed to incubate for 1 h to facilitate the methoxy groups of both APTMS and PTMS to react with the silanol group on the SiNW surface to form the APTMS/SiNW-FET. The chip was washed again with ethanol, blown dry with N_2, and cured at 110 °C for 5 min. The mixture of APTMS and PTMS (1:5) allows for the ability to control the density of the aptamers on the SiNW-FET surface to ensure enough space for the proper folding of the aptamers in association with the target molecules. On average, only ∼15% of the SiNW surface contains APTMS as the active sites (amine groups) to be modified with the aptamers. Apart from controlling the density of the aptamers on the SiNW-FET surface, the PTMS also provides a

Figure 1. Experimental setup for detecting K$^+$ ions with the aptamer/SiNW-FETs. (a) Schematic illustration of using the aptamer/SiNW-FETs for detecting the K$^+$ ions released from cultured cortical neurons. The MPC SiNW-FET devices were modified with K$^+$-specific DNA-aptamers (referred to as aptamer/SiNW-FETs). The neurons grown on a coverslip were placed to contact the aptamer/SiNW-FETs encompassed by a PDMS wall. A Pt electrode was used as a solution gate and was kept at ground potential during the electrical measurements. Upon stimulation, the K$^+$ ions released from the cortical neurons bind the aptamer/SiNW-FETs to induce a conductance change inside the MPC SiNW-FETs. (b) Process of modifying the aptamers on the MPC SiNW-FETs (details in the Experimental Section). We first modified the SiNW surfaces with 3-aminopropyltrimethoxysilane (APTMS) and propyltrimethoxysilane (PTMS) at a ratio of 1:5. We then chose N,N'-disuccinimidyl carbonate (DSC) as a chemical linker to react the amino group of APTMS at one end and to immobilize the K$^+$-specific DNA-aptamer at the other end (via the reaction with the amino group attached on the 5′-terminal of the aptamer). The drawing is not to scale.
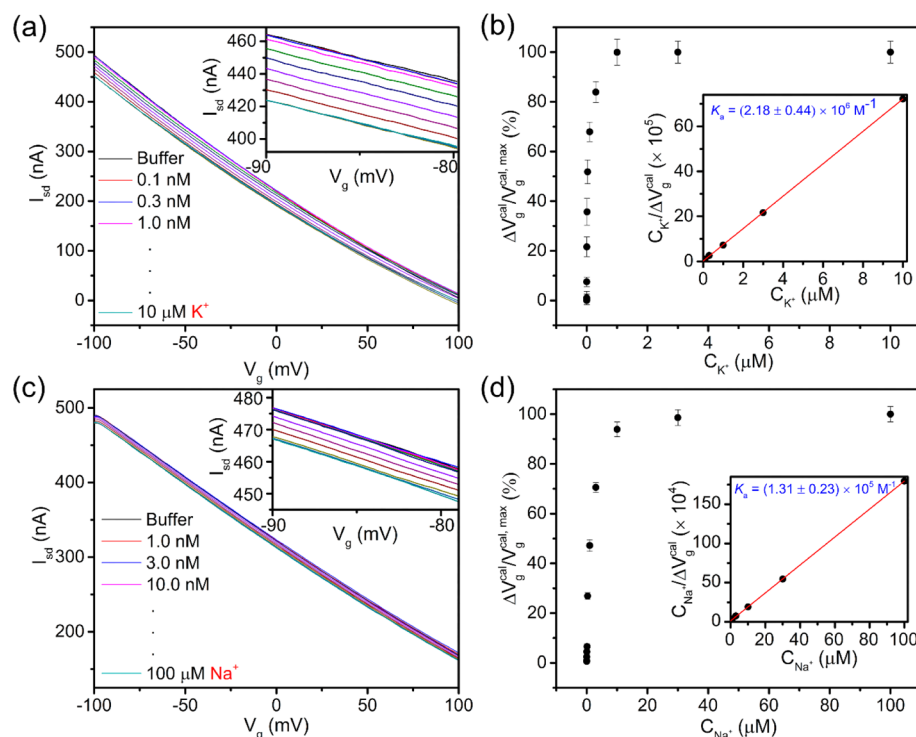
chemically inert surface to prevent nonspecific binding in the biosensing experiments.

A solution containing 5 mg N,N'-disuccinimidyl carbonate (DSC, acting as a chemical linker to immobilize the DNA-aptamers on the APTMS/SiNW-FET) in 15 μL of N,N-diisopropylethylamine (DIPEA) and 1.5 mL of anhydrous dimethyl sulfoxide (DMSO) was prepared, and of that, a drop was placed on the APTMS/SiNW-FET chip for a 2 h reaction. Prior to immobilizing the DNA-aptamers (a 27-mer sequence of NH$_2$-5′-ACCTGGGGGGAGTATTGCGGAGGAA-GGT-3′ synthesized by MDBio), the chip was washed twice with anhydrous DMSO and was then immersed in an aqueous solution containing the DNA-aptamers (1 μM) for 2 h to form the aptamer/SiNW-FETs. The chip was washed again with DI water and blown dry with N$_2$ gas. To demonstrate that the DNA-aptamers could be successfully immobilized on the SiO$_2$/Si surface, we used a fluorescein isothiocyanate (FITC)-tagged aptamer with an amino group attached on the 5′-terminal (i.e., 5′-NH$_2$-TTTTTTT-FITC-3′, referred to as FITC-aptamer) to show that the FITC-aptamers could be uniformly immobilized on a SiO$_2$/Si substrate via the chemical linkers of DSC and APTMS (Figure S2a). A homogeneous fluorescence image

indicates the uniform modification of the FITC-aptamers on the SiO$_2$/Si surface. The modification of the DNA-aptamers on an MPC SiNW-FET was also examined by measuring the shifts in the $I_{sd}-V_g$ curves. As depicted in Figure S2b, the shift of the $I_{sd}-V_g$ curve after the DNA-aptamer modification was caused by a gating effect on the MPC SiNW-FET due to the negatively charged backbone of the DNA-aptamer, consequently increasing the electrical conductance of the p-type MPC SiNW-FET.

Electrical Measurement. The $I_{sd}-V_g$ measurements of the aptamer/SiNW-FETs were acquired with a lock-in amplifier (Stanford Research System, SR830) operated at a $V_{sd} = 10$ mV, a modulation frequency of 79 Hz, and a time constant of 100 ms. For the detection of the metal cations by the aptamer/SiNW-FET, different sample concentrations were dissolved in a 10 mM Tris buffer solution at pH 7.4 (with the Debye−Hückel length of ∼9.6 nm) to effectively detect signals without causing severe electrolytic screening. The sample solution was either dropped directly onto the aptamer/SiNW-FET chip with a PDMS wall (Figure 1a) or delivered to the aptamer/SiNW-FET devices through a PDMS microfluidic channel (L 6.26 mm × W 500 μm × H 50 μm) driven by a syringe pump (KD Scientific,

Figure 2. Detection of the alkali cations (K^+ or Na^+) by the aptamer/SiNW-FET. The plots in (a) and (c) present the $I_{sd}-V_g$ curves measured with an aptamer/SiNW-FET in response to different C_{K^+} and C_{Na^+}, respectively. The insets show the expanded scale at $V_g = -90$ to -80 mV. (b) and (d) present the normalized $\Delta V_g^{cal}/\Delta V_g^{cal,max}$ (where $\Delta V_g^{cal,max}$ is the saturated ΔV_g^{cal}) as a function of C_{K^+} and C_{Na^+}, respectively. The insets show a least-squares fit of the measured data points to the Langmuir adsorption isotherm model to yield association constants of forming the aptamer-K^+ complex ($K_a = (2.18 \pm 0.44) \times 10^6$ M^{-1}) and the aptamer-Na^+ complex ($K_a = (1.31 \pm 0.23) \times 10^5$ M^{-1}). The experimental data presented in (b) and (d) are the mean $\pm$ the standard deviation and $n = 3$ measurements.

KD-101). A Pt electrode, immersed in the sample solution throughout the sensing experiment, was used as a solution gate with the voltage supplied by a DAQ system (National Instruments, DAQ-NI2110) and was maintained at ground potential to minimize the electrical noise in the system. After each sensing experiment, the metal cations captured by aptamer/SiNW-FET were washed off by flushing Tris buffer through the PDMS microfluidic channel to return the aptamer/SiNW-FET device to its original state without any binding metal cations.

Primary Culture of Cortical Neurons. A pregnant Sprague–Dawley rat was anesthetized and the E14.5 embryos were isolated as described previously.[36] The procedure complied with the Animal Welfare Regulations and was approved by the Institutional Animal Care and Use Committee (Permit No. 103–30), National Taiwan University. In brief, the dissected cortex was digested with papain and recovered in a cold Ca^{2+} and Mg^{2+} free Hank's balanced salt solution (Ca^{2+}/Mg^{2+}-free HBSS, containing 5.33 mM KCl, 0.44 mM KH_2PO_4, 0.5 mM, 138 mM NaCl, 4 mM $NaHCO_3$, 0.3 mM Na_2HPO_4, and 5.6 mM glucose, pH 7.4). The solution containing the neurons was centrifuged under 168× g for 3 min at 4 °C, and the pellet was resuspended in Neurobasal medium supplemented with B27 (Invitrogen). The cells were plated on 24 mm poly(L-lysine) coated coverslips at a density of 3×10^6 cell/mL. The neurons were placed in a humidified CO_2 (5%) incubator, and the medium was replaced every other day. For the electrical measurements with the aptamer/SiNW-FETs, a neuron-seeded coverslip was placed atop an aptamer/SiNW-FET device leading the cultured neurons to contact the device surface. Prior to the cell experiments, the neuron-seeded coverslip was washed with the NMG buffer twice to remove the adhering culture media.

Electrophysiology Recording. The whole-cell voltage- and current-clamp recordings were performed at room temperature (22–25 °C) with an EPC-10 amplifier and the Pulse program (HEKA Elektronik, Germany, v 8.7) as described previously.[37] The cells were incubated in the NMG buffer, and the pipet solution for the recordings contained 120 mM aspartic acid, 5 mM $MgCl_2$, 40 mM HEPES, 0.1

mM EGTA, 2 mM ATP, and 0.3 mM GTP, pH 7.3 with KOH (310 mOsm/kg). After achieving a whole-cell configuration, the cells were held at −70 mV for 5 min to ensure the stability of the seal. The patched cells were stimulated with AMPA (10 μM in the NMG buffer) ejected from a micropipette with an opening of ~1 μm positioned 15 μm from the patched neurons.

■ RESULTS AND DISCUSSION

A schematic representation of using an aptamer/SiNW-FET for detecting the K^+ ions released from cultured cortical neurons is illustrated in Figure 1. The MPC SiNW-FET device comprises hundreds of p-type single-crystalline SiNWs (~20 nm in diameter each) as conducting channels, which are connected by interdigitated source and drain electrodes (Figure 1a and details in Figure S1a−b of the Supporting Information (SI)). The device fabrication and the electrical measurements are described in Experimental Section.[23] The MPC SiNW-FETs possess an ohmic contact at a source-drain bias voltage (V_{sd}) of −200−200 mV (Figure S1b) and a high transconductance of >1200 nS measured at $V_{sd} = 10$ mV in 1× PBS solution, pH 7.4 (Figure S1c). Compared with the traditional SiNW-FET, which has only a single or a few SiNW(s) as a conducting channel, the MPC SiNW-FET possesses a remarkably higher detection sensitivity (i.e., larger transconductance) resulting in an enhanced signal-to-noise ratio (SNR) in electrical measurements.

As suggested by Rajan et al.,[38] the intrinsic quality of an SiNW-FET device is the major contribution to the SNR during electrical measurements; other factors, such as pH, electrolyte concentration, and composition, play a minor role. The MPC SiNW-FET design composed of hundreds of SiNWs could

reduce the device-to-device variation, because the noise is a weighted average of the fluctuations from individual SiNWs of discrete dopant concentration.[39,40] For the SiNW-FETs with a single SiNW as a conducting channel, the transconductance might be smaller than the MPC SiNW-FETs, but the noise could be minimized by a carefully tuned circuit and be reduced by the interference from other SiNWs of low wire quality that might occur in an MPC SiNW-FET. Overall, the MPC design provides a convenient and stable circuit for SiNW-FETs and improves the SNR by enhancing the driving current response.[39,40]

The DNA-aptamer chosen for K$^+$ sensing was an oligonucleotide with a sequence of 5′-ACCTGGGGGAGTAT-TGCGGAGGAAGGT-3′ (27-mer)[41] that was immobilized on an MPC SiNW-FET (as described in Figure 1b and Figure S2). It is worth noting that in the immobilization of the K$^+$-specific aptamers on the SiNW-FET surface, the number density of the aptamers was controlled by a mixture (1:5) of 3-amino-propyltrimethoxysilane (APTMS) and propyltrimethoxysilane (PTMS) to ensure enough space for the proper folding of the aptamers in binding with the K$^+$ ions. When the aptamer/SiNW-FET captures K$^+$ ions, the electrical conductance in the FET device is altered, which can be read from the shift in a source-drain current vs gate voltage (I_{sd}–V_g) curve or from the variation in a real-time (I_{sd}–t) measurement. In our experiments, the electrical measurements of the SiNW-FETs were conducted with a lock-in amplifier, and a solution gate voltage was supplied by a data acquisition (DAQ) system through a platinum (Pt) electrode.[14,42−44]
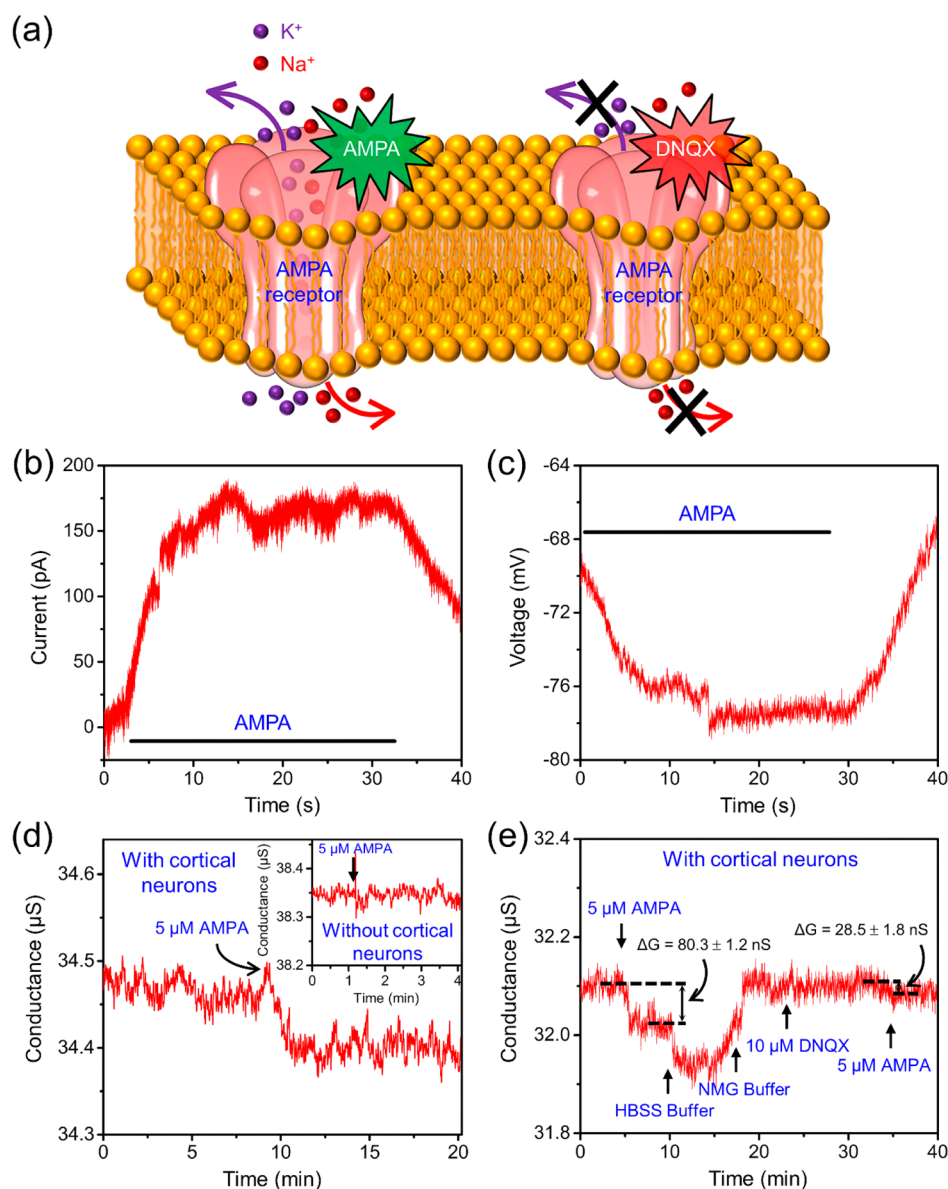
To evaluate the sensitivity of the aptamer/SiNW-FETs for detecting K$^+$, we perfused different C_{K^+} in 10 mM Tris buffer (pH 7.4) through a polydimethylsiloxane (PDMS) microfluidic channel, which was coupled to the aptamer/SiNW-FET device. Figure 2a plots the measured I_{sd}–V_g curves of an aptamer/SiNW-FET in response to various C_{K^+} at 10^{-10}–10^{-5} M, and the I_{sd}–V_g curves shift downward as C_{K^+} increases, indicating the p-type characteristics of the aptamer/SiNW-FET device. To have a correct interpretation of the electrical measurements despite device-to-device variations, we converted the current changes caused by receptor-target binding (ΔI_{sd} at a certain V_g relative to the buffer solution) to the changes in V_g (termed "calibrated response"), which were represented by ΔV_g^{cal} according to the I_{sd}–V_g transfer curve of the FET device used (as shown in Figure S3).[23,45] Figure 2b shows the calibrated response of $\Delta V_{g, K^+}^{cal}$ as a function of C_{K^+}, of which the data were converted from Figure 2a at $V_g = -90$ mV where the I_{sd}–V_g curves are almost linear and the ΔI_{sd} values are significant. The $\Delta V_{g, K^+}^{cal}/\Delta V_{g, K^+}^{cal, max}$ value shown in Figure 2b increases as C_{K^+} increases and reaches a plateau at $C_{K^+} > 1$ μM (i.e., $\Delta V_{g, K^+}^{cal, max}$, the saturated $\Delta V_{g, K^+}^{cal}$). To calculate the association constant (K_a) of forming the aptamer-K$^+$ complex, we plotted the $C_{K^+}/\Delta V_{g, K^+}^{cal}$ against C_{K^+} (in the inset of Figure 2b) and had a least-squares fit to the Langmuir adsorption isotherm model (Section S2 of the SI). The association constant of the aptamer-K$^+$ complex was determined to be $K_a = (2.18 \pm 0.44) \times 10^6$ M^{-1}, which is close to an earlier report of 2.5×10^6 M^{-1}.[41] In the K$^+$-sensing measurements with the aptamer/SiNW-FETs, the nonspecific binding of K$^+$ was tested with a control experiment by employing a PTMS-modified SiNW-FET (referred to as PTMS/SiNW-FET) without immobilizing the K$^+$-specific DNA-aptamer. The resultant I_{sd}–V_g curves, measured by PTMS/SiNW-FET (Figure S4a), showed no apparent response to K$^+$ at $C_{K^+} = 10^{-10}$–10^{-5} M,

which was in sharp contrast to the prominent conductance changes detected by the aptamer/SiNW-FET (Figure 2a,b and Figure S4b).

Figure 2c shows the I_{sd}–V_g curves of the same aptamer/SiNW-FET device in reaction to different C_{Na^+} at 10^{-9}–10^{-4} M. The inset shows that Na$^+$ has less of a gating effect than K$^+$ to the aptamer/SiNW-FET (in shifting the I_{sd}–V_g curves downward). The normalized $\Delta V_{g, Na^+}^{cal}/\Delta V_{g, Na^+}^{cal, max}$ against C_{Na^+} are plotted in Figure 2d where the $K_a = (1.31 \pm 0.23) \times 10^5$ M^{-1} of forming the aptamer-Na$^+$ complex was obtained from a least-squares fit. These results reveal that the affinity of the aptamer to K$^+$ is approximately 17-fold greater compared with Na$^+$, indicating that most of the G-quadruplexes also have a binding affinity to Na$^+$ albeit much less than to K$^+$.[46] With further tests, this aptamer/SiNW-FET device exhibited very low affinities to Li$^+$, Cs$^+$, and Ca^{2+} (Figure S5), and consequently, this aptamer/SiNW-FET device is suitable for sensing K$^+$ in biological buffers. The linear working range of detecting K$^+$ by the aptamer/SiNW-FET spanned from 10^{-9} to 10^{-6} M (Figure S6), and the limit of detection of ~10^{-9} M was generally better than those of several previously reported G-quadruplex-based K$^+$ sensors (Table S1). Consequently, this sensory device is suitable for sensing minute changes in C_{K^+} in a buffer containing various biological ions.

Biological samples usually contain both K$^+$ and Na$^+$ ions with different ratios, but the total concentrations are about the same to maintain a constant osmolarity. The presence of Na$^+$ will interfere the aptamer/SiNW-FET in sensing K$^+$, although the FET sensor favors the binding to K$^+$ by 17 times over Na$^+$. To verify that the aptamer/SiNW-FET can respond to K$^+$ in the presence of Na$^+$ under the same total ionic strength, we prepared solutions containing a mixture of K$^+$ and Na$^+$ in different concentration ratios and kept the ionic strength of the analyte solutions constant throughout the measurements (K$^+$:Na$^+$ = 0:10, 1:9, 3:7, 5:5, 7:3, 9:1, and 10:0, units in μM). As shown in Figure S7a, an increase in the K$^+$ ratio of the K$^+$-Na$^+$ mixture induced a further downward shift of the I_{sd}–V_g curves, and after converting to the ΔV_g^{cal}, the calibrated plot shows a linear response as the proportion of K$^+$ increases (Figure S7b). This linear response reveals that the conductance changes of the aptamer/SiNW-FET are mostly attributed to C_{K^+}, which can be applied to the C_{K^+} measure from a biological mixture, especially when C_{K^+} is higher than C_{Na^+}.

According to the electrochemical gradient of K$^+$ ions in live cells, K$^+$ ions usually flow out of a cell and shift the membrane potential negatively to modulate the excitability of a neuron. Therefore, the opening of K$^+$-related channels at the plasma membrane leads to K$^+$ efflux, thus increasing the local $C_{K^+}^{ex}$ despite the difficulty of measuring this local change. To demonstrate the capability of an aptamer/SiNW-FET in detecting the released K$^+$ ions from live cells, we placed cortical neurons grown on a coverslip atop the aptamer/SiNW-FET with the neurons facing the device and stimulated the neurons with AMPA dissolved in a Na$^+$/K$^+$-free N-methyl-D-glucamine (NMG) buffer (containing 150 mM NMG, 5 mM glucose, 10 mM 4-(2-Hydroxyethyl)piperazine-1-ethanesul-fonic acid (HEPES), 1 mM MgCl$_2$·6H$_2$O, and 2.2 mM CaCl$_2$·2H$_2$O, pH 7.4). It should be noted that we omitted Na$^+$ from the bath solution here to avoid the interference of the Na$^+$ ions (usually present in a normal physiological buffer) in binding to the aptamer/SiNW-FETs. The AMPA targets a class of ionotropic glutamate receptors, i.e., an AMPA receptor (AMPAR), which mediates a fast synaptic transmission in the
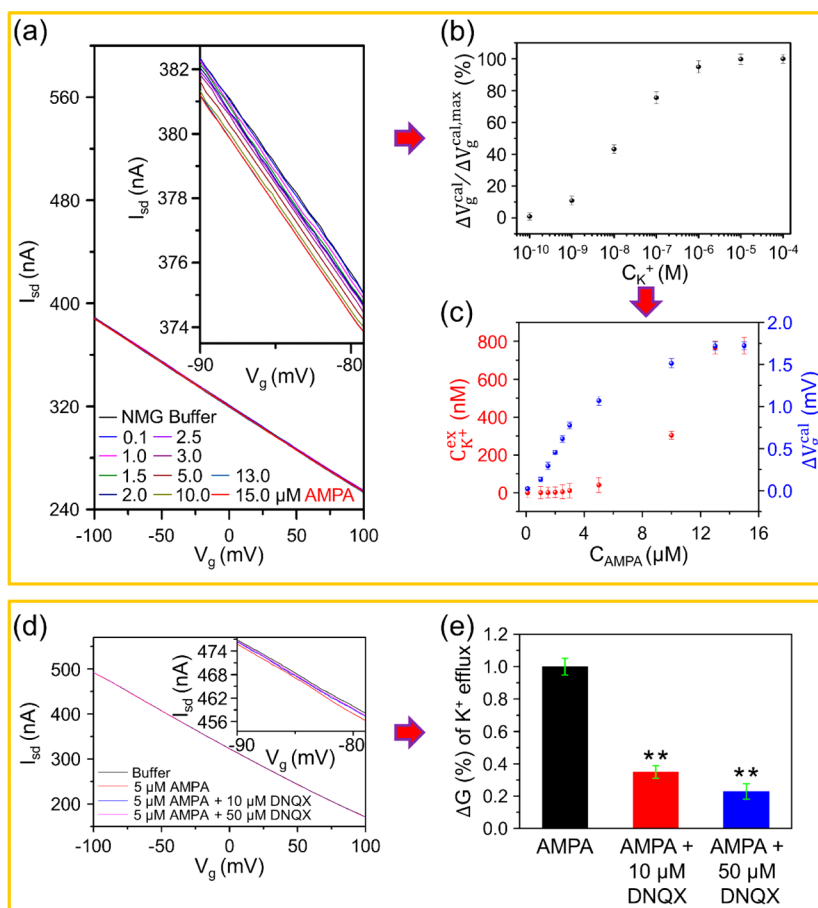
Figure 3. AMPA stimulation induces an outward current in cortical neurons and elevates $C_{K^+}^{ex}$. (a) Illustration of the activation and inhibition of an AMPA receptor (AMPAR). The binding of AMPA to an AMPAR activates the conjugated ion channel to flux Na^+ and K^+ across the membrane according to their respective electrochemical concentration gradients. DNQX, a competitive antagonist of AMPA, prevents the binding of AMPA to the AMPAR resulting in the inhibition of the channel activation. (b,c) AMPA-induced electric responses from a patched cortical neuron. A neuron incubated in Na^+/K^+-free NMG buffer was whole-cell patched in voltage-clamp (b) and current-clamp (c) modes to measure the ionic current and the membrane potential evoked by AMPA (10 μM), respectively. (d) Electrical responses of an aptamer/SiNW-FET to the K^+ efflux from AMPA-stimulated cortical neurons. Neurons grown on a coverslip were placed atop the aptamer/SiNW-FET and were stimulated with 5 μM AMPA in a Na^+/K^+-free NMG buffer. The conductance change of the aptamer/SiNW-FET was monitored in a real-time mode. The inset shows a control test without cortical neurons. (e) Effect of DNQX. Neurons were treated with 5 μM AMPA (to induce ΔG = 80.3 ± 1.2 nS) and then were washed with HBSS and the NMG buffer. After a 10 μM DNQX incubation, 5 μM AMPA was added again in the presence of DNQX to stimulate the neurons (to cause ΔG = 28.5 ± 1.8 nS).

central nervous system.[47] As illustrated in Figure 3a, the activation of the AMPAR allows the inward Na^+ and outward K^+ fluxes of a cell under a normal physiological condition and shifts the membrane potential positively and negatively, respectively. Figure 3b shows the recording from a whole-cell patched neuron in a voltage-clamp mode with a holding potential of −70 mV, where the AMPA (10 μM, dissolved in NMG buffer) stimulation evoked a transient outward current of ~150 pA and then was gradually inactivated. By changing the recording to a current-clamp mode to monitor the membrane potential (Figure 3c), the AMPA stimulation hyperpolarized

the membrane potential. These patch-clamp data suggest that AMPA induces an outward K^+ current to hyperpolarize the membrane potential from cortical neurons in the Na^+/K^+-free NMG buffer.

To verify that the flow of K^+ from the cytosol to the external milieu changes the local $C_{K^+}^{ex}$, we placed a coverslip seeded with cortical neurons (the experimental details are described in the Experimental Section) in contact with the aptamer/SiNW-FET and monitored the conductance change in Na^+/K^+-free NMG buffer. Figure 3d shows that a decreased conductance (SNR > 3) in the aptamer/SiNW-FET was observed under AMPA
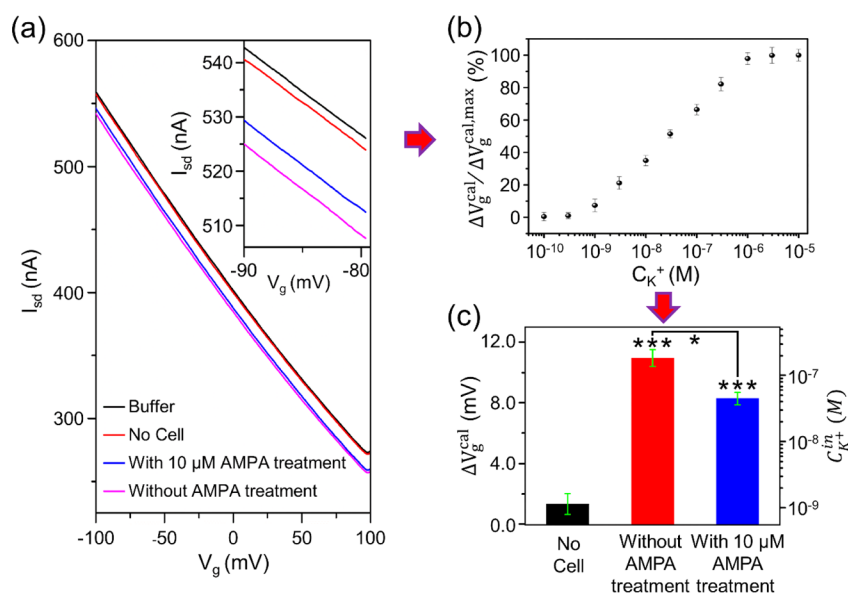
Figure 4. Cultured cortical neurons exhibit an elevated $C_{K^+}^{ex}$ under AMPA stimulation. Neurons grown on the glass coverslips were placed atop of the aptamer/SiNW-FET and were stimulated with AMPA of different concentrations. The electric responses of an aptamer/SiNW-FET to the K^+ efflux from the stimulated neurons were monitored. (a) The I_{sd}–V_g curves were measured from the neurons stimulated with C_{AMPA} = 0–15 μM in the NMG buffer at pH 7.4. (b) Calibration curve. Prior to the experiment in (a), a calibration curve of ΔV_g^{cal} vs C_{K^+} for the aptamer/SiNW-FET was performed. (c) $C_{K^+}^{ex}$ in the vicinity of neurons as recorded by the aptamer/SiNW-FET. The ΔV_g^{cal} (right ordinate, blue circles) obtained with the data from (a) was converted to $C_{K^+}^{ex}$ (left ordinate, red circles) according to the calibration curve in (b). (d) The I_{sd}–V_g curves measured from the neurons pretreated with DNQX. Neurons were pretreated with DNQX (10 or 50 μM) 10 min before the application of AMPA (10 μM) and the electric responses of the aptamer/SiNW-FET were recorded. (e) Normalized changes in the electrical conductance (ΔG) of the aptamer/SiNW-FET. Data presented were the mean ± the standard deviation from at least 3 batches of neurons and the significance was analyzed by Student's t-test. **, $p <$ 0.01 when compared with the neurons treated with AMPA only.

stimulation, demonstrating the release of K^+ from the neuron cells. In contrast, the inset of Figure 3d presents a control experiment where AMPA had no electrical effect on the aptamer/SiNW-FET without the presence of cells. To further confirm that AMPAR was involved in the AMPA-induced conductance change, we pretreated the neurons with 10 μM 6,7-dinitroquinoxaline-2,3-dione (DNQX, an antagonist of AMPAR), and subsequently, the AMPA-induced conductance change was suppressed by ∼65% (Figure 3e). As a consequence, these results demonstrate that the minute release of K^+ from neurons increases the $C_{K^+}^{ex}$ (to a level of ∼10^{-7}–10^{-6} M as will be shown later) which could be detected by the sensitive aptamer/SiNW-FET.

The amount of neurotransmitters released from the presynaptic neuron determines the number of receptors activated at the postsynaptic neuron. To characterize that the changes in $C_{K^+}^{ex}$ are determined by the concentration of AMPA (C_{AMPA}) applied, we perfused the aptamer/SiNW-FET in the presence of cortical neurons with different C_{AMPA} (0.1, 1, 1.5, 2, 2.5, 3, 5, 10, 13, and 15 μM) and measured the electric responses in Na^+/K^+-free NMG buffer (Figure 4a). The results

show that the electric response increased as C_{AMPA} increased. To convert the electric response to C_{K^+}, we calibrated the ΔV_g^{cal} as a function of C_{K^+} (Figure 4b), which was conducted prior to the cell experiment using the same aptamer/SiNW-FET. Through the calibration curve, we plotted the $C_{K^+}^{ex}$ (whose amount was reflected by ΔV_g^{cal} of the aptamer/SiNW-FET) as a function of C_{AMPA} (Figure 4c), where the $C_{K^+}^{ex}$ increased from a basal level under 50 nM at a $C_{AMPA} <$ 2.5 μM to a plateau of ∼800 nM at a $C_{AMPA} >$ 13 μM. The 50% effective concentration (EC_{50}) of AMPA for elevating $C_{K^+}^{ex}$ was 10.3 μM, which was slightly lower than what was reported before by measuring the dose-dependent AMPA current (17 μM).[48] This difference might be due to the low capacity of the aptamer/SiNW-FET device. When $C_{K^+} >$ 1 μM, the ΔV_g^{cal} reaches a saturation level at ∼1.8 mV (Figure 4b); however, when $C_{AMPA} >$ 13 μM, the ΔV_g^{cal} is ∼1.7 mV (Figure 4c) which is almost at the maximal ΔV_g^{cal} level that this device could respond. Henceforth, even though high C_{AMPA} activates more AMPA channels to elevate the $C_{K^+}^{ex}$, the response of the aptamer/SiNW-FET is already saturated resulting in an underestimation of the EC_{50}.

Figure 5. Cortical neurons reveal the declining $C_{K^+}^{in}$ under AMPA stimulation. (a) The $I_{sd}-V_g$ curves measured from the diluted cytosolic solutions. The cytosolic solutions, collected from the neurons with or without AMPA stimulation, were diluted with the NMG buffer for the aptamer/SiNW-FET measurements (details in Section S4). (b) Calibration curve. Prior to the experiment in (a), a calibration curve of ΔV_g^{cal} vs C_{K^+} of this aptamer/SiNW-FET was conducted. (c) Calibrated $C_{K^+}^{in}$ in diluted samples. The ΔV_g^{cal} (left ordinate) obtained from different solutions in (a) was converted to $C_{K^+}^{in}$ (right ordinate) according to the calibration curve in (b). Data presented were the mean ± the standard deviation; the significance was analyzed by Student's t-test. * $p < 0.05$, *** $p < 0.001$.

To further confirm that the AMPA-induced conductance changes were mediated by the AMPAR, we pretreated the neurons with DNQX, an antagonist of AMPAR, before the AMPA stimulation. Figure 4d illustrates the $I_{sd}-V_g$ curves obtained by pretreating the neurons with different C_{DNQX}(10 and 50 μM) and subsequently exposing the neurons to 5 μM of AMPA. The DNQX pretreatment decreased the AMPA-induced $C_{K^+}^{ex}$ as evidenced by the reduced downward shifts of the $I_{sd}-V_g$ curves. The normalized conductance changes (Figure 4e) revealed that 10 and 50 μM DNQX pretreatments significantly inhibited the 5 μM AMPA-induced conductance changes to only 35 ± 4% ($n = 3$, $p < 0.05$) and 21 ± 5% ($n = 3$, $p < 0.05$), respectively. DNQX is a competitive inhibitor of AMPA with a half maximal inhibitory concentration of ~500 nM.[49] As a result, the effectiveness of DNQX at suppressing the AMPA-evoked response suggests that AMPAR is involved in the AMPA-evoked conductance change.

The AMPA-evoked K$^+$ efflux should increase $C_{K^+}^{ex}$ and decrease the intracellular C_{K^+}($C_{K^+}^{in}$) simultaneously. To measure the $C_{K^+}^{in}$ remaining in the neurons after the 10 μM AMPA treatment, we stimulated ~10^6 neurons suspended in 0.5 mL of a normal bath buffer containing Na$^+$. After stimulation, neurons were washed with NMG buffer and lysed as described in section S4. The cytosolic fraction was then dissolved in 0.5 mL of NMG buffer and diluted by 1000× for aptamer/SiNW-FET measurements (Figure 5a). Briefly, three solutions were prepared (1) from the medium containing no neuron cells, (2) from the neurons without AMPA treatment, and (3) from the neurons with the 10 μM AMPA treatment. Figure 5a shows the shifted $I_{sd}-V_g$ curves of the aptamer/SiNW-FET tested by the three solutions with the same amounts of lysates. Without or with AMPA treatment, the ΔV_g^{cal} values of the lysates prepared from the neurons after the 1000× dilution were 10.96 ± 0.55 and 8.30 ± 0.41 mV, respectively, corresponding to $C_{K^+}^{in}$ = 220 ± 20 and 54 ± 4 nM (Figure 5c) via the calibration (Figure 5b). Although the SiNW-FET devices used in Figures

2, 4, and 5 were different, the semilog calibration curves of normalized $\Delta V_g^{cal}/\Delta V_g^{cal,max}$ against C_{K^+} shown in Figures 4b, 5b, and S6 revealed that these aptamer-modified devices all have a linear working range of C_{K^+} between 10^{-5} and 10^{-9} M. To obtain a consistent result in measuring the C_{K^+} when using different devices, we prepared a calibration curve every time before the start of an experiment.

Supposing that the radius of a neuron is 10 μm; the deduced cytosolic $C_{K^+}^{in}$ was approximately 26.3 and 6.4 mM in the neurons, respectively, without or with the AMPA stimulation (Section S4). The $C_{K^+}^{in}$ values obtained were much lower than what is generally accepted of a $C_{K^+}^{in} \sim 140$ mM. There are several assumptions, which may underestimate the conversion, such as the survival of neurons, the loss of K$^+$ during preparation, and the size of neurons. Despite these factors, our results clearly demonstrate that the $C_{K^+}^{in}$ is reduced by 75% (i.e., 220 ± 20 nM vs 54 ± 4 nM) after the AMPA stimulation under the same preparation procedure (Figure 5c) which hints that the $C_{K^+}^{in}$ could be greatly reduced under strong stimulation, such as epilepsy; in the meantime, such a large amount of K$^+$ fluxes out of the cell would elevate the $C_{K^+}^{ex}$. Henceforth, these concomitant changes in the K$^+$ concentrations across the membrane would shift the membrane potential toward zero and enhance the neuron excitability.

Under normal physiological conditions, the activation of AMPAR allows the influx of Na$^+$ and thus depolarizes the membrane potential to activate the voltage-gated Na$^+$ channels for action potential generation. This depolarization then activates the voltage-gated K$^+$ channels resulting in an outward K$^+$ current which could reach several nanoamperes, in cortical neurons to repolarize the membrane potential. By model simulation, the accumulation of K$^+$ in the interstitial fluid, due to the repeated action-potential firings from one neuron, can induce synchronized firings from nearby neurons.[50] This effect is even more pronounced in a neuron network, where many factors, such as gap junctions, Na$^+$/K$^+$-ATPase, and K$^+$ currents,

work cooperatively to modulate the K^+ lateral diffusion and create a K^+ environment that is optimal for the generation and propagation of action potentials.[51] Normally, the $C_{K^+}^{ex}$ ranges over 2−5 mM in the human cerebral microdialysate[52] and can reach even 55 mM in the cortex during ischemia or epilepsy.[53,54] The glial syncytium spatial buffering mechanism disperses the local $C_{K^+}^{ex}$ surge by translocating K^+ from the sites of elevated $C_{K^+}^{ex}$ to those of lower $C_{K^+}^{ex}$.[55,56] It is estimated that 80% of the K^+ released by neurons would be sequestered by glia cells in less than 10 s, resulting in returning the $C_{K^+}^{ex}$ and neuronal excitability to the basal level.[57] Therefore, the comprehending $C_{K^+}^{ex}$ dynamics provides the necessary information for understanding the interactions among neurons in a network.

Although we measured the $C_{K^+}^{ex}$ from neurons incubated in a Na^+/K^+-free NMG buffer to block the generation of action potential and the activation of voltage-gated K^+ channels, our results clearly showed that AMPA could elicit a significant change in the conductance of SiNW-FET in a dose-dependent manner. As shown in Figure 3b and c, the AMPA stimulation elicited only a small outward K^+ current of ∼100 pA and hyperpolarized the membrane potential. In addition, the $C_{K^+}^{ex}$ monitored in this experiment is an average of the local environment; because of the diffusion, the actual $C_{K^+}^{ex}$ under physiological buffer should be much higher in the vicinity of cellular plasma membrane than we detected in this report. Therefore, by improving the selectivity of the receptor molecules modified on an MPC SiNW-FET, we could then perform the same experiment using a normal physiological buffer to estimate the $C_{K^+}^{ex}$ under different stimulations. In this study, DNQX of different concentrations attenuated the AMPA-evoked conductance change to various levels; henceforth, instead of measuring the AMPA-evoked current by an electrophysiological technique, we could use this aptamer/SiNW-FET device to monitor the minute K^+ efflux through the AMPAR in the intact-cell mode to characterize the physiological activities of the AMPAR. The whole-cell patch-clamp technique is a powerful tool for measuring the electric activities of ion channels; however, it interferes the intracellular content and is not appropriate for characterizing the effect of the intracellular signaling pathway.[58] In this work, by measuring the K^+ released from the intact cells with MPC SiNW-FETs, we could verify how the channels are modulated by various signaling pathways.

Finally, this aptamer/SiNW-FET has a 17-fold K^+ selectivity over Na^+ and is able to sense K^+ ions from a mixture even with Na^+ ions in the background (Figure S7). For biological samples of a $K^+−Na^+$ mixture, such as the cytosolic fraction that has a C_{K^+} higher than a C_{Na^+}, the changes in C_{K^+} can be detected and quantitated by the aptamer/SiNW-FET upon proper calibration.

Each unit of the MPC SiNW-FET with interdigitated electrodes has dimensions of 40 μm × 90 μm. With a sensor of this size, we could not monitor the C_{K^+} at the surface of a cell, but the C_{K^+} effluxed from a group of cells at the vicinity of the circuit. Therefore, the diffusion of the accumulated K^+ ions from the cell surface to the MPC SiNW-FETs determines the response time in the experiment. An ion-selective electrode (ISE) coated with a specific ion exchanger material or membrane could have good ion selectivity to detect the concentrations of ions accumulated in the buffer; however, due to the small tip diameter (0.5−1.0 μm) and the exchanger material used, ISE has a high resistance ranging from 10^9 to 10^{11} Ω.[59−61] Therefore, users must take special precautions, such as cable connection, signal grounding, and electrical input impedance of the signal amplifiers, to promise a tiny current for the measurements. As the progress of nanotechnology, we could reduce the size of MPC SiNW-FETs and exploit the advantages of the nanowires to detect the K^+ at a small region, such as the cell surface.[62−64]

■ CONCLUSIONS

In conclusion, we demonstrate that an aptamer/SiNW-FET is a reliable sensor for detecting K^+ with high sensitivity in real-time and with label-free capability. As the fast progress in nanotechnology, the size of MPC SiNW-FETs used in this report could further be reduced for the detection of biological activities at subcellular domains. With the target selectivity and the detection sensitivity of an aptamer against various cations, the aptamer/SiNW-FET is able to monitor the target ions, such as the K^+ in this study, released from living neuron cells. Our results reveal that even a small K^+ efflux from a group of neurons induces a significant $C_{K^+}^{ex}$ elevation; in addition, the $C_{K^+}^{in}$ decreases significantly when stimulated under normal physiological buffer. These suggest a substantial change in $C_{K^+}^{ex}$ during repetitive or strong neuronal activities, and the concomitant C_{K^+} change on both sides of the plasma membrane would in turn enhance the neuron excitability. With this sensory device, we also measured the C_{K^+} from different biological samples to characterize physiological activities, such as the effects of the voltage-gated K^+ channels on intracellular and extracellular C_{K^+}, neurotransmission, and so forth. Therefore, by selecting an appropriate aptamer, the aptamer/SiNW-FET serves as a useful biosensor that can detect the concentration changes of various biological molecules released from live cells under different physiological conditions.

■ ASSOCIATED CONTENT

Ⓢ Supporting Information

The Supporting Information is available free of charge on the ACS Publications website at DOI: 10.1021/acssensors.6b00505.

> Materials and Reagents (S1), Association Constant (S2), Estimation of IC_{50} values using a Boltzmann sigmoidal function (S3), Determination of K^+ from cellular extract (S4), Comparison of the limits of detection among various G-quadruplex-based K^+ biosensors (Table S1), Electrical characterization of a representative MPC SiNW-FET device (Figure S1), Demonstration of the successful immobilization of DNA-aptamers on SiO_2/Si surface (Figure S2), Calibration of an aptamer/SiNW-FET to avoid device-to-device variation in the detection sensitivity with different FETs (Figure S3), Comparative responses of a PTMS/SiNW-FET and an aptamer/SiNW-FET to different C_{K^+} (Figure S4), Target-selectivity of an aptamer/SiNW-FET against various biologically relevant ions (Figure S5), Linear working range of this aptamer/SiNW-FET device (Figure S6), Aptamer/SiNW-FET senses K^+ ions in the presence of Na^+ ions (Figure S7) (PDF)

■ AUTHOR INFORMATION

Corresponding Authors
*E-mail: cypan@ntu.edu.tw.
*E-mail: ytcchem@ntu.edu.tw.

ORCID ⓘ

Yit-Tsong Chen: 0000-0002-6204-8320

Notes

■ REFERENCES

(1) Terker, A. S.; Zhang, C.; McCormick, J. A.; Lazelle, R. A.; Zhang, C.; Meermeier, N. P.; Siler, D. A.; Park, H. J.; Fu, Y.; Cohen, D. M.; Weinstein, A. M.; Wang, W.-H.; Yang, C.-L.; Ellison, D. H. Potassium Modulates Electrolyte Balance and Blood Pressure through Effects on Distal Cell Voltage and Chloride. *Cell Metab.* **2015**, *21*, 39−50.

(2) Adler, S.; Fraley, D. S. Potassium and Intracellular pH. *Kidney Int.* **1977**, *11*, 433−442.

(3) Yu, S. P. Regulation and Critical Role of Potassium Homeostasis in Apoptosis. *Prog. Neurobiol.* **2003**, *70*, 363−386.

(4) Doyle, D. A.; Cabral, J. M.; Pfuetzner, R. A.; Kuo, A.; Gulbis, J. M.; Cohen, S. L.; Chait, B. T.; MacKinnon, R. The Structure of the Potassium Channel: Molecular Basis of K⁺ Conduction and Selectivity. *Science* **1998**, *280*, 69−77.

(5) Grob, D.; Liljestrand, Ä.; Johns, R. J. Potassium Movement in Normal Subjects: Effect on Muscle Function. *Am. J. Med.* **1957**, *23*, 340−355.

(6) Bean, B. P. The Action Potential in Mammalian Central Neurons. *Nat. Rev. Neurosci.* **2007**, *8*, 451−465.

(7) Nicholson, C.; Syková, E. Extracellular Space Structure Revealed by Diffusion Analysis. *Trends Neurosci.* **1998**, *21*, 207−215.

(8) Cui, Y.; Wei, Q.; Park, H.; Lieber, C. M. Nanowire Nanosensors for Highly Sensitive and Selective Detection of Biological and Chemical Species. *Science* **2001**, *293*, 1289−1292.

(9) Stern, E.; Klemic, J. F.; Routenberg, D. A.; Wyrembak, P. N.; Turner-Evans, D. B.; Hamilton, A. D.; LaVan, D. A.; Fahmy, T. M.; Reed, M. A. Label-Free Immunodetection with CMOS-Compatible Semiconducting Nanowires. *Nature* **2007**, *445*, 519−522.

(10) Pui, T.-S.; Agarwal, A.; Ye, F.; Huang, Y.; Chen, P. Nanoelectronic Detection of Triggered Secretion of Pro-Inflammatory Cytokines Using CMOS Compatible Silicon Nanowires. *Biosens. Bioelectron.* **2011**, *26*, 2746−2750.

(11) Gao, A.; Lu, N.; Dai, P.; Li, T.; Pei, H.; Gao, X.; Gong, Y.; Wang, Y.; Fan, C. Silicon-Nanowire-Based CMOS-Compatible Field-Effect Transistor Nanosensors for Ultrasensitive Electrical Detection of Nucleic Acids. *Nano Lett.* **2011**, *11*, 3974−3978.

(12) Zhang, G.-J.; Huang, M. J.; Ang, J. A. J.; Yao, Q.; Ning, Y. Label-Free Detection of Carbohydrate−Protein Interactions Using Nanoscale Field-Effect Transistor Biosensors. *Anal. Chem.* **2013**, *85*, 4392−4397.

(13) Wang, Y.; Wang, T.; Da, P.; Xu, M.; Wu, H.; Zheng, G. Silicon Nanowires for Biosensing, Energy Storage, and Conversion. *Adv. Mater.* **2013**, *25*, 5177−5195.

(14) Kim, J.; Rim, Y. S.; Chen, H.; Cao, H. H.; Nakatsuka, N.; Hinton, H. L.; Zhao, C.; Andrews, A. M.; Yang, Y.; Weiss, P. S. Fabrication of High-Performance Ultrathin In₂O₃ Film Field-Effect Transistors and Biosensors Using Chemical Lift-Off Lithography. *ACS Nano* **2015**, *9*, 4572−4582.

(15) Lin, S.-P.; Pan, C.-Y.; Tseng, K.-C.; Lin, M.-C.; Chen, C.-D.; Tsai, C.-C.; Yu, S.-H.; Sun, Y.-C.; Lin, T.-W.; Chen, Y.-T. A Reversible Surface Functionalized Nanowire Transistor to Study Protein−Protein Interactions. *Nano Today* **2009**, *4*, 235−243.

(16) Lin, T.-W.; Hsieh, P.-J.; Lin, C.-L.; Fang, Y.-Y.; Yang, J.-X.; Tsai, C.-C.; Chiang, P.-L.; Pan, C.-Y.; Chen, Y.-T. Label-Free Detection of

(17) Pui, T.-S.; Agarwal, A.; Ye, F.; Tou, Z.-Q.; Huang, Y.; Chen, P. Ultra-Sensitive Detection of Adipocytokines With CMOS-Compatible Silicon Nanowire Arrays. *Nanoscale* **2009**, *1*, 159−163.

(18) Gao, A.; Lu, N.; Wang, Y.; Dai, P.; Li, T.; Gao, X.; Wang, Y.; Fan, C. Enhanced Sensing of Nucleic Acids with Silicon Nanowire Field Effect Transistor Biosensors. *Nano Lett.* **2012**, *12*, 5262−5268.

(19) Chang, K.-S.; Sun, C.-J.; Chiang, P.-L.; Chou, A.-C.; Lin, M.-C.; Liang, C.; Hung, H.-H.; Yeh, Y.-H.; Chen, C.-D.; Pan, C.-Y.; Chen, Y.-T. Monitoring Extracellular K⁺ Flux With a Valinomycin-Coated Silicon Nanowire Field-Effect Transistor. *Biosens. Bioelectron.* **2012**, *31*, 137−143.

(20) Gao, X. P. A.; Zheng, G.; Lieber, C. M. Subthreshold Regime has the Optimal Sensitivity for Nanowire FET Biosensors. *Nano Lett.* **2010**, *10*, 547−552.

(21) Zheng, G.; Gao, X. P. A.; Lieber, C. M. Frequency Domain Detection of Biomolecules Using Silicon Nanowire Biosensors. *Nano Lett.* **2010**, *10*, 3179−3183.

(22) Li, B.-R.; Chen, C.-W.; Yang, W.-L.; Lin, T.-Y.; Pan, C.-Y.; Chen, Y.-T. Biomolecular Recognition With a Sensitivity-Enhanced Nanowire Transistor Biosensor. *Biosens. Bioelectron.* **2013**, *45*, 252−259.

(23) Li, B.-R.; Hsieh, Y.-J.; Chen, Y.-X.; Chung, Y.-T.; Pan, C.-Y.; Chen, Y.-T. An Ultrasensitive Nanowire-Transistor Biosensor for Detecting Dopamine Release from Living PC12 Cells under Hypoxic Stimulation. *J. Am. Chem. Soc.* **2013**, *135*, 16034−16037.

(24) Moyzis, R. K.; Buckingham, J. M.; Cram, L. S.; Dani, M.; Deaven, L. L.; Jones, M. D.; Meyne, J.; Ratliff, R. L.; Wu, J. R. A Highly Conserved Repetitive DNA Sequence, (TTAGGG)N, Present at the Telomeres of Human Chromosomes. *Proc. Natl. Acad. Sci. U. S. A.* **1988**, *85*, 6622−6626.

(25) Parkinson, G. N.; Lee, M. P. H.; Neidle, S. Crystal Structure of Parallel Quadruplexes from Human Telomeric DNA. *Nature* **2002**, *417*, 876−880.

(26) Keefe, A. D.; Pai, S.; Ellington, A. Aptamers As Therapeutics. *Nat. Rev. Drug Discovery* **2010**, *9*, 537−550.

(27) Suess, B.; Hanson, S.; Berens, C.; Fink, B.; Schroeder, R.; Hillen, W. Conditional Gene Expression by Controlling Translation with Tetracycline-Binding Aptamers. *Nucleic Acids Res.* **2003**, *31*, 1853−1858.

(28) Chen, K.-I.; Li, B.-R.; Chen, Y.-T. Silicon Nanowire Field-Effect Transistor-Based Biosensors for Biomedical Diagnosis and Cellular Recording Investigation. *Nano Today* **2011**, *6*, 131−154.

(29) He, F.; Tang, Y.; Wang, S.; Li, Y.; Zhu, D. Fluorescent Amplifying Recognition for DNA G-Quadruplex Folding with a Cationic Conjugated Polymer: A Platform for Homogeneous Potassium Detection. *J. Am. Chem. Soc.* **2005**, *127*, 12343−12346.

(30) Wang, L.; Liu, X.; Hu, X.; Song, S.; Fan, C. Unmodified Gold Nanoparticles As a Colorimetric Probe for Potassium DNA Aptamers. *Chem. Commun.* **2006**, *36*, 3780−3782.

(31) Radi, A.-E.; O'Sullivan, C. K. Aptamer Conformational Switch As Sensitive Electrochemical Biosensor for Potassium Ion Recognition. *Chem. Commun.* **2006**, *32*, 3432−3434.

(32) Vassanelli, S.; Fromherz, P. Transistor Probes Local Potassium Conductances in the Adhesion Region of Cultured Rat Hippocampal Neurons. *J. Neurosci.* **1999**, *19*, 6767−6773.

(33) Wrobel, G.; Seifert, R.; Ingebrandt, S.; Enderlein, J.; Ecken, H.; Baumann, A.; Kaupp, U. B.; Offenhäusser, A. Cell-Transistor Coupling: Investigation of Potassium Currents Recorded with p- and n-Channel FETs. *Biophys. J.* **2005**, *89*, 3628−3638.

(34) Ingebrandt, S.; Yeung, C.-K.; Krause, M.; Offenhäusser, A. Neuron−Transistor Coupling: Interpretation of Individual Extracellular Recorded Signals. *Eur. Biophys. J.* **2005**, *34*, 144−154.

(35) Patolsky, F.; Zheng, G.; Lieber, C. M. Fabrication of Silicon Nanowire Devices for Ultrasensitive, Label-Free, Real-Time Detection of Biological and Chemical Species. *Nat. Protoc.* **2006**, *1*, 1711−1724.

(36) Wu, M.-P.; Kao, L.-S.; Liao, H.-T.; Pan, C.-Y. Reverse Mode Na⁺/Ca²⁺ Exchangers Trigger the Release of Ca²⁺ from Intracellular

Ca²⁺ Stores in Cultured Rat Embryonic Cortical Neurons. *Brain Res.* **2008**, *1201*, 41−51.

(37) Chou, M.-Y.; Lee, C.-Y.; Liou, H.-H.; Pan, C.-Y. Phenytoin Attenuates the Hyper-Exciting Neurotransmission in Cultured Embryonic Cortical Neurons. *Neuropharmacology* **2014**, *83*, 54−61.

(38) Rajan, N. K.; Routenberg, D. A.; Reed, M. A. Optimal Signal-To-Noise Ratio for Silicon Nanowire Biochemical Sensors. *Appl. Phys. Lett.* **2011**, *98*, 264107.

(39) Regonda, S.; Tian, R.; Gao, J.; Greene, S.; Ding, J.; Hu, W. Silicon Multi-Nanochannel FETs to Improve Device Uniformity/Stability and Femtomolar Detection of Insulin in Serum. *Biosens. Bioelectron.* **2013**, *45*, 245−51.

(40) Accastelli, E.; Scarbolo, P.; Ernst, T.; Palestri, P.; Selmi, L.; Guiducci, C. Multi-Wire Tri-Gate Silicon Nanowires Reaching Milli-pH Unit Resolution in One Micron Square Footprint. *Biosensors* **2016**, *6*, 9.

(41) Huang, C.-C.; Chang, H.-T. Aptamer-Based Fluorescence Sensor for Rapid Detection of Potassium Ions in Urine. *Chem. Commun.* **2008**, *12*, 1461−1463.

(42) Tang, X.; Bansaruntip, S.; Nakayama, N.; Yenilmez, E.; Chang, Y. I.; Wang, Q. Carbon Nanotube DNA Sensor and Sensing Mechanism. *Nano Lett.* **2006**, *6*, 1632−1636.

(43) A platinum (Pt) electrode is suitable for our experiments, because the electrode fouling is not an issue for the Pt electrode to be used in the medium containing a Tris buffer with K⁺ ions. Moreover, a Pt electrode shows excellent reproducibility of the electrode potential during the course of electrical measurements. Comparatively, a commonly used Ag/AgCl reference electrode is not suitable, because the Ag⁺ ions have tendency to form complexes in the Tris buffer, thereby clogging the junction and resulting in substantial "liquid junction" potentials across it (ref 44).

(44) Troutman, T.; Prasauckas, K. A.; Kennedy, M. A.; Stevens, J.; Davies, M. G.; Dadd, A. T. In *Molecular Biology Problem Solver: A Laboratory Guide*; Gerstein, A. S, Ed.; Wiley: New York, 2001; p 85.

(45) Ishikawa, F. N.; Curreli, M.; Chang, H.-K.; Chen, P.-C.; Zhang, R.; Cote, R. J.; Thompson, M. E.; Zhou, C. A Calibration Method for Nanowire Biosensors to Suppress Device-to-Device Variation. *ACS Nano* **2009**, *3*, 3969−3976.

(46) Nojima, T.; Ueyama, H.; Takagi, M.; Takenaka, S. Potassium Sensing Oligonucleotide, PSO, Based on DNA Tetraplex Formation. *Nucleic Acids Symp. Ser.* **2002**, *2*, 125−126.

(47) Mayer, M. L. Glutamate Receptor Ion Channels. *Curr. Opin. Neurobiol.* **2005**, *15*, 282−288.

(48) Dai, W.-M.; Egebjerg, J.; Lambert, J. D. C. Characteristics of AMPA Receptor-Mediated Responses of Cultured Cortical and Spinal Cord Neurones and their Correlation to the Eexpression of Glutamate Receptor Subunits, GluR1−4. *Br. J. Pharmacol.* **2001**, *132*, 1859−1875.

(49) Jane, D. E.; Hoo, K.; Kamboj, R.; Deverill, M.; Bleakman, D.; Mandelzys, A. Synthesis of Willardiine and 6-Azawillardiine Analogs: Pharmacological Characterization on Cloned Homomeric Human AMPA and Kainate Receptor Subtypes. *J. Med. Chem.* **1997**, *40*, 3645−3650.

(50) Bazhenov, M.; Timofeev, I.; Steriade, M.; Sejnowski, T. J. Potassium Model for Slow (2−3 Hz) In Vivo Neocortical Paroxysmal Oscillations. *J. Neurophysiol.* **2004**, *92*, 1116−1132.

(51) Wu, X.-X.; Shuai, J. Effects of Extracellular Potassium Diffusion on Electrically Coupled Neuron Networks. *Phys. Rev. E* **2015**, *91*, 022712.

(52) Antunes, A.; Schiefecker, A.; Beer, R.; Pfausler, B.; Sohm, F.; Fischer, M.; Dietmann, A.; Lackner, P.; Hackl, W.; Ndayisaba, J.-P.; Thomé, C.; Schmutzhard, E.; Helbok, R. Higher Brain Extracellular Potassium is Associated with Brain Metabolic Distress and Poor Outcome After Aneurysmal Subarachnoid Hemorrhage. *Crit. Care* **2014**, *18*, R119.

(53) Hansen, A. J.; Zeuthen, T. Extracellular Ion Concentrations During Spreading Depression and Ischemia in the Rat Brain Cortex. *Acta Physiol. Scand.* **1981**, *113*, 437−445.

(54) Gabriel, S.; Eilers, A.; Kivi, A.; Kovacs, R.; Schulze, K.; Lehmann, T. N.; Heinemann, U. Effects of Barium on Stimulus Induced Changes in Extracellular Potassium Concentration in Area CA1 of Hippocampal Slices from Normal and Pilocarpine-Treated Epileptic Rats. *Neurosci. Lett.* **1998**, *242*, 9−12.

(55) Kofuji, P.; Newman, E. A. Potassium Buffering in the Central Nervous System. *Neuroscience* **2004**, *129*, 1043−1054.

(56) Newman, E.; Frambach, D.; Odette, L. Control of Extracellular Potassium Levels by Retinal Glial Cell K⁺ Siphoning. *Science* **1984**, *225*, 1174−1175.

(57) Sibille, J.; Dao, D. K.; Holcman, D.; Rouach, N. The Neuroglial Potassium Cycle During Neurotransmission: Role of Kir4.1 Channels. *PLoS Comput. Biol.* **2015**, *11*, e1004137.

(58) Marty, A.; Zimmerberg, J. Diffusion into the Patch-Clamp Recording Pipette of a Factor Necessary for Muscarinic Current Response. *Cell. Signalling* **1989**, *1*, 259−68.

(59) Mu, L.; Chang, Y.; Sawtelle, S. D.; Wipf, M.; Duan, X.; Reed, M. A. Silicon Nanowire Field-Effect Transistors − A Versatile Class of Potentiometric Nanobiosensors. *IEEE Access* **2015**, *3*, 287−302.

(60) Morf, W. E.; Simon, W. In *Ion-Selective Electrodes in Analytical Chemistry*; Freiser, H., Ed.; 1st ed.; Plenum Press: New York, 1980; pp 169−170.

(61) Haemmerli, A.; Janata, J.; Brown, H. M. In *Progress in Enzyme and Ion-Selective Electrodes*; Lübbers, D. W.; Acker, H.; Buck, R. P.; Eisenman, G.; Kessler, M.; Simon, W., Eds.; 1st ed.; Springer Verlag: Berlin Heidelberg, 1981; p 46.

(62) Grieshaber, D.; MacKenzie, R.; Vörös, J.; Reimhult, E. Electrochemical Biosensors - Sensor Principles and Architectures. *Sensors* **2008**, *8*, 1400−1458.

(63) Dai, X.; Zhou, W.; Gao, T.; Liu, J.; Lieber, C. M. Three-Dimensional Mapping and Regulation of Action Potential Propagation in Nanoelectronics-Innervated Tissues. *Nat. Nanotechnol.* **2016**, *11*, 776.

(64) Qing, Q.; Jiang, Z.; Xu, L.; Gao, R.; Mai, L.; Lieber, C. M. Free-Standing Kinked Nanowire Transistor Probes for Targeted Intracellular Recording in Three Dimensions. *Nat. Nanotechnol.* **2013**, *9*, 142−147.

Supporting Information

Detection of K⁺ Efflux from Stimulated Cortical Neurons by an Aptamer-Modified Silicon Nanowire Field-Effect Transistor

Ankur Anand,[†,‡,§] Chia-Rung Liu,[§,⊥] Ai-Chuan Chou,[∥] Wan-Hsuan Hsu,[∥] Rajesh Kumar Ulaganathan,[†,§,⊥] Yi-Cheng Lin,[#] Chi-An Dai,[#] Fan-Gang Tseng,[‡] Chien-Yuan Pan,[∥,*] and Yit-Tsong Chen[§,⊥,*]

[†]Nanoscience and Technology Program, Taiwan International Graduate Program, Academia Sinica, Taipei 115, Taiwan

[‡]Department of Engineering and System Science, National Tsing Hua University, Hsinchu 30013, Taiwan

[§]Institute of Atomic and Molecular Sciences, Academia Sinica, Taipei 106, Taiwan

[∥]Department of Life Science, National Taiwan University, Taipei 106, Taiwan,

[⊥]Department of Chemistry, National Taiwan University, Taipei 106, Taiwan

[#]Department of Chemical Engineering, National Taiwan University, Taipei 106, Taiwan

*Address correspondence to cypan@ntu.edu.tw, ytcchem@ntu.edu.tw

Table of Contents

S1. Materials and Reagents

Trizma hydrochloride (Tris-HCl), 3-aminopropyltrimethoxysilane (APTMS), propyltrimethoxysilane (PTMS), dimethyl sulfoxide (DMSO), *N,N*-diisopropylethylamine (DIPEA), and *N,N'*-disuccinimidyl carbonate (DSC) were purchased from Sigma-Aldrich. Other chemicals were also purchased commercially: single-strain DNA-aptamer from MDBio, polydimethylsiloxane (PDMS) from Sil-More Industrial, and Hank's balanced salt solution (HBSS) from Gibco. Dulbecco's modified Eagle's medium and all other reagents for cell culture were purchased from Invitrogen. Deionized (DI) water (>18 MΩ·cm) obtained from a purification system (Millipore Synergy) was used throughout the experiments.

S2. Association Constant

The association constant (K_a) of forming the aptamer-K^+ complex was determined by a least-squares fit of the $\Delta V_{g,K^+}^{cal} - C_{K^+}$ data (the inset of Figure 2b) to the Langmüir adsorption isotherm model[S1]

$$\frac{C_{K^+}}{\Delta V_{g,K^+}^{cal}} = \frac{1}{\Delta V_{g,K^+}^{cal,max}} \cdot C_{K^+} + \frac{1}{\Delta V_{g,K^+}^{cal,max}} \cdot \frac{1}{K_a} \qquad \text{(Eq. S1)}$$

where the relative $\Delta V_{g,K^+}^{cal}$ is defined as $\Delta V_{g,K^+}^{cal}$ (%) = $(\Delta V_{g,K^+}^{cal} - \Delta V_{g,0}^{cal}) / \Delta V_{g,0}^{cal} \times 100$ (%), $\Delta V_{g,K^+}^{cal}$ is the calibrated response at C_{K^+} = 0 M that induces no detectable signal, and $\Delta V_{g,K^+}^{cal,max}$ is the saturated calibrated response at high C_{K^+}.

S3. Estimation of IC$_{50}$ Values Using a Boltzmann Sigmoidal Function

The IC$_{50}$ value was determined by fitting the dose response curve (Figure 4c) to a Boltzmann sigmoidal function with Origin 9.1 (OriginLab, 120 Northampton, MA).

$$y = \frac{A_1 - A_2}{1 + e^{\frac{(x - x_o)}{dx}}} + A_2 \qquad \text{(Eq. S2)}$$

where, A_1, and A_2 are the values of the lower and upper limits on the dose-response curve, respectively, x is the AMPA concentration, x_0 is the dose corresponding to the midpoint (*i.e.*, IC_{50}) between A_1 and A_2, and dx denotes the slope of the dose-response curve.

S4. Determination of K^+ from Cellular Extract

A sample of 500 µL freshly isolated cortical neurons suspension containing ~10^6 cells was added in Hank's balanced salt solution (HBSS, 137 mM NaCl, 5.4 mM KCl, 0.25 mM Na_2HPO_4, 0.1 g glucose, 0.44 mM KH_2PO_4, 1.3 mM $CaCl_2$, 1.0 mM $MgSO_4$, 4.2 mM $NaHCO_3$, pH 7.4) buffer. The cells were treated with 10 µM AMPA in HBSS for 10 min and then centrifuged; the pellet was then resuspended in 500 µL of the NMG buffer to remove the stimulant and extracellular K^+. The neurons were centrifuged and then resuspended followed sequentially by washing with NMG buffer containing 4 % (v/v) paraformaldehyde for 15 min to fix the neurons. Thereafter, the cells were centrifuged and resuspended in 500 µL of the NMG buffer containing 0.5 % Triton X-100 solution for 30 min at a constant shaking condition. Subsequently, the lysed neurons were centrifuged and the supernatant was collected. The supernatant was diluted (1000×) with the NMG buffer for the following experiments. The control solution was obtained with the same procedure but without the AMPA treatment to the cells.

The C_{K^+} values of the diluted cytosolic fractions for the control and the AMPA-treated neurons were 220 and 54 nM, respectively; before the 1000× dilution, the C_{K^+} values were 220 and 54 µM, which were equivalent to 0.11 and 0.027 mol K^+ in 0.5 mL solution. We pooled the cytosolic fraction from 10^6 cells and assumed that each neuron has a radius of 10 µm; therefore, the total volume of the cells is 4.2 µL for each sample. Consequently, the $C_{K^+}^{in}$ is 26.3 mM (6.4 mM) in neurons without (with) the AMPA treatment.
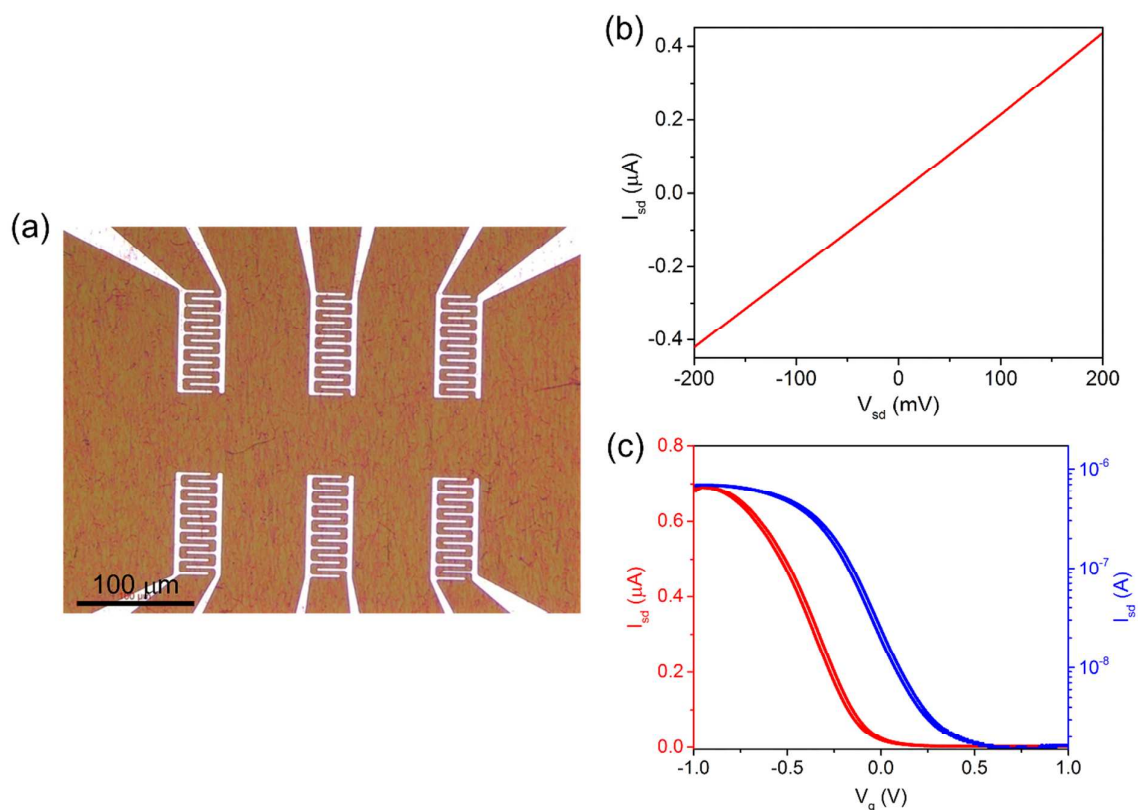
Table S1. Comparison of the Limits of Detection among Various G-quadruplex-based K$^+$ Biosensors

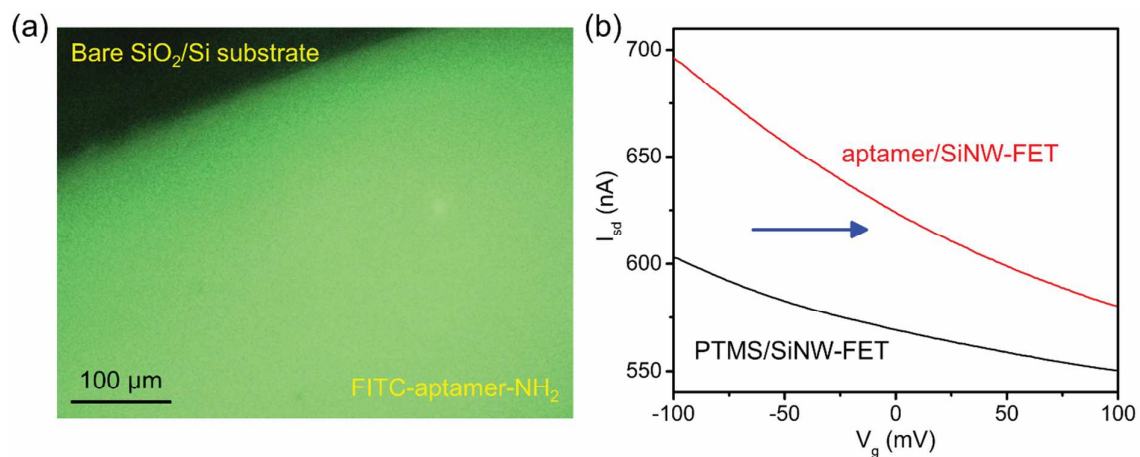| Method	Technique	LOD^a	Linear range	Reference
Electrical	Field-effect transistor	1 nM	1 nM – 1 µM	This Work
Optical	Fluorescence	31 nM	0 – 1.6 mM	[S2]
Optical	Fluorescence	900 nM	4 µM – 1 mM	[S3]
Optical	Fluorescence	2 µM	5 µM – 1 mM	[S4]
Optical	Fluorescence	2.5 µM	2.5 µM – 5 mM	[S5]
Optical	Fluorescence	400 µM	600 µM – 20 mM	[S6]
Optical	Absorption	1.9 nM	10 nM – 10 mM	[S7]
Optical	Colorimetry	5 nM	5 nM – 1 µM	[S8]
Electrochemical	SWV^b	0.1 nM	0.1 nM – 50 nM	[S9]
Electrochemical	SWV^b	2.31 nM	10 nM – 10 µM	[S10]
Electrochemical	SWV^b	50 nM	50 nM – 1 mM	[S11]
Electrochemical	CV^c	1.6 µM	5 µM – 200 µM	[S12]

^{a} LOD: limit of detection.

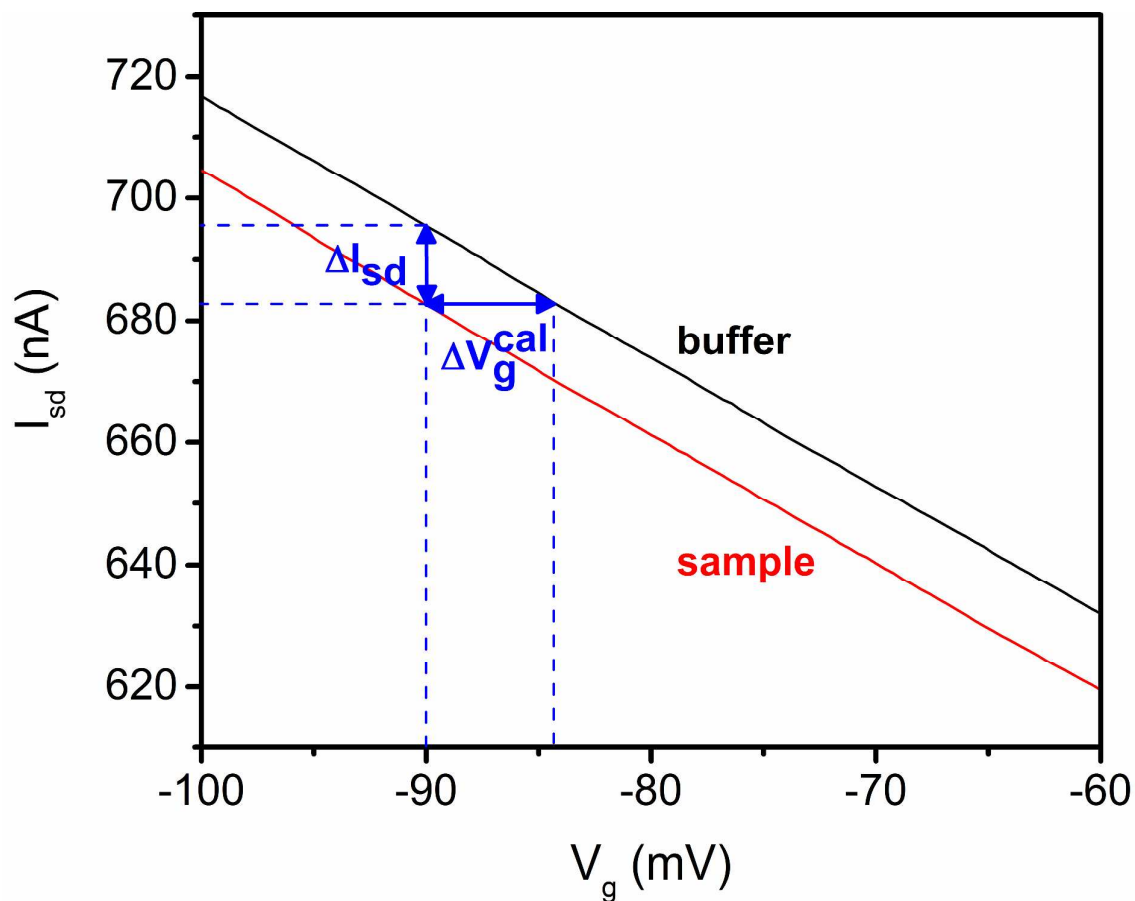^{b} SWV: Square wave voltammetry.

^{c} CV: cyclic voltammetry.

Figure S1. Electrical characterization of a representative MPC SiNW-FET device. (a) A device chip contains six sets of MPC SiNW-FETs. Every MPC SiNW-FET set comprises hundreds of p-type single-crystalline SiNWs (~20 nm in diameter each) as conducting channels, which are connected by interdigitated source and drain electrodes. For a particular experiment, measurement was done using one set of MPC-SiNW FET. Scale bar is 100 μm. (b) A representative plot of the measured I_{sd}–V_{sd} curve shows that the MPC SiNW-FETs formed ohmic contacts. The I_{sd}–V_{sd} curves were scanned in ambient condition with a digital multimeter (Keithley 6487). (c) The I_{sd}–V_g curve of a bare MPC SiNW-FET was measured in 1× PBS buffer solution (containing 10 mM Na_2HPO_4, 1.8 mM KH_2PO_4, 137 mM NaCl, and 2.7 mM KCl, at pH 7.4) using a lock-in amplifier (Stanford Research System, SR830) at V_{sd} of 10 mV, a modulation frequency of 79 Hz, and a time constant of 100 ms. The solution gate voltage (V_g), scanned from -1 V to +1 V and back to -1 V, was applied to a Ag/AgCl reference electrode via a DAQ system. The obtained I_{sd}–V_g curve is plotted on linear (red) and logarithmic (blue) scales.
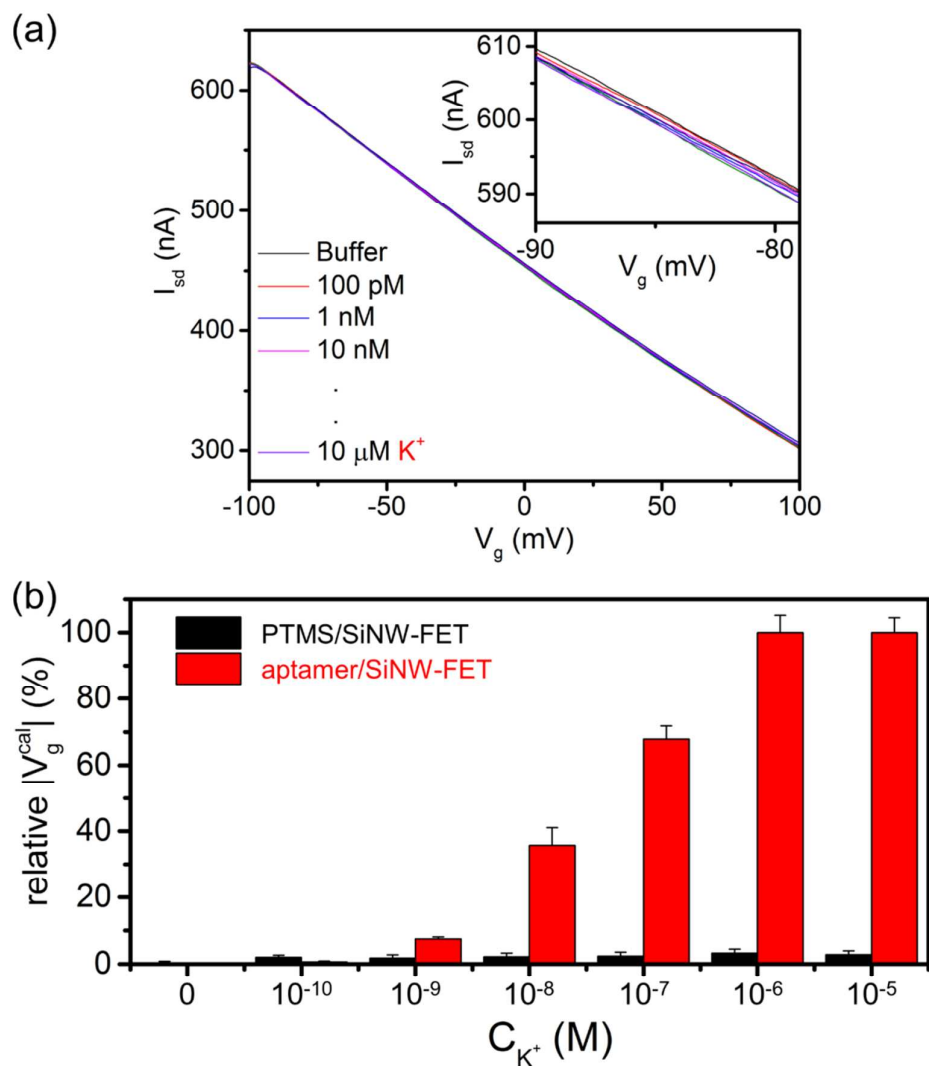
Figure S2. Demonstration of the successful immobilization of DNA-aptamers on SiO$_2$/Si surface. (a) Fluorescent image of an FITC-aptamer-modified SiO$_2$/Si substrate. The modification procedures are the same as those described in Figure 1b and the Materials and Methods. Scale bar is 100 µm. (b) The I$_{sd}$–V$_g$ curves recorded from a PTMS/SiNW-FET (black trace) and an aptamer/SiNW-FET (red trace) in a 10 mM Tris buffer.
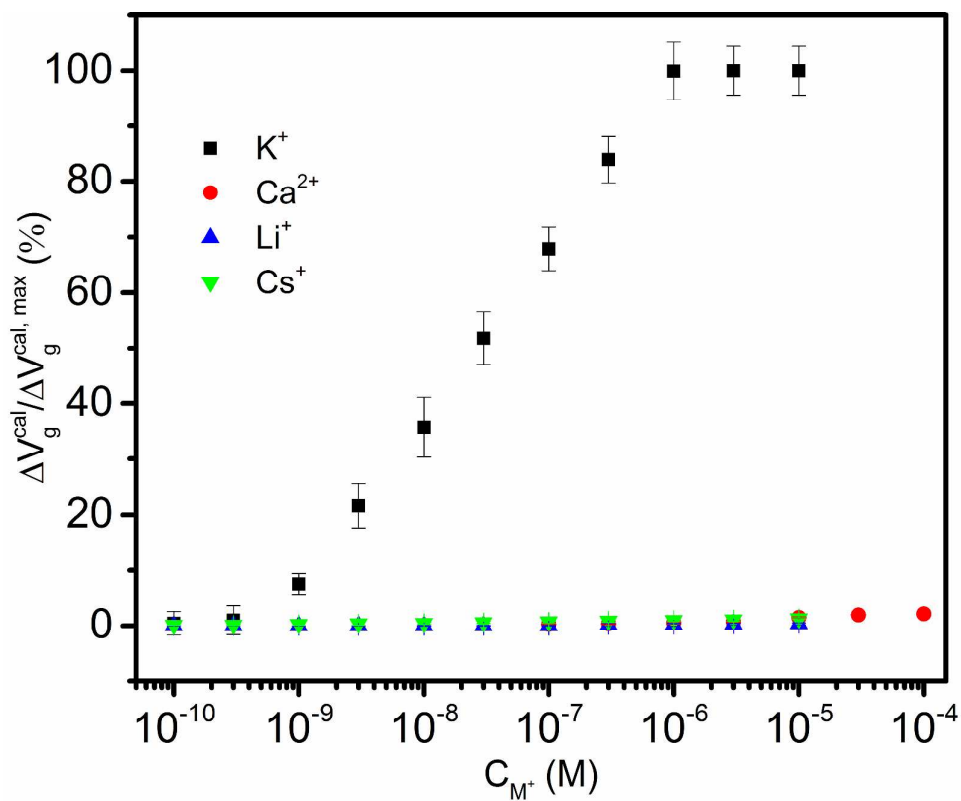
Figure S3. To avoid device-to-device variation in the detection sensitivity with different FETs, the measured current change due to the receptor-target binding (ΔI_{sd} at V_g = -90 mV, relative to the buffer solution) was converted to the changes in V_g (termed the calibrated response and represented by ΔV_g^{cal}) according to the I_{sd}–V_g transfer curve of the FET device used.
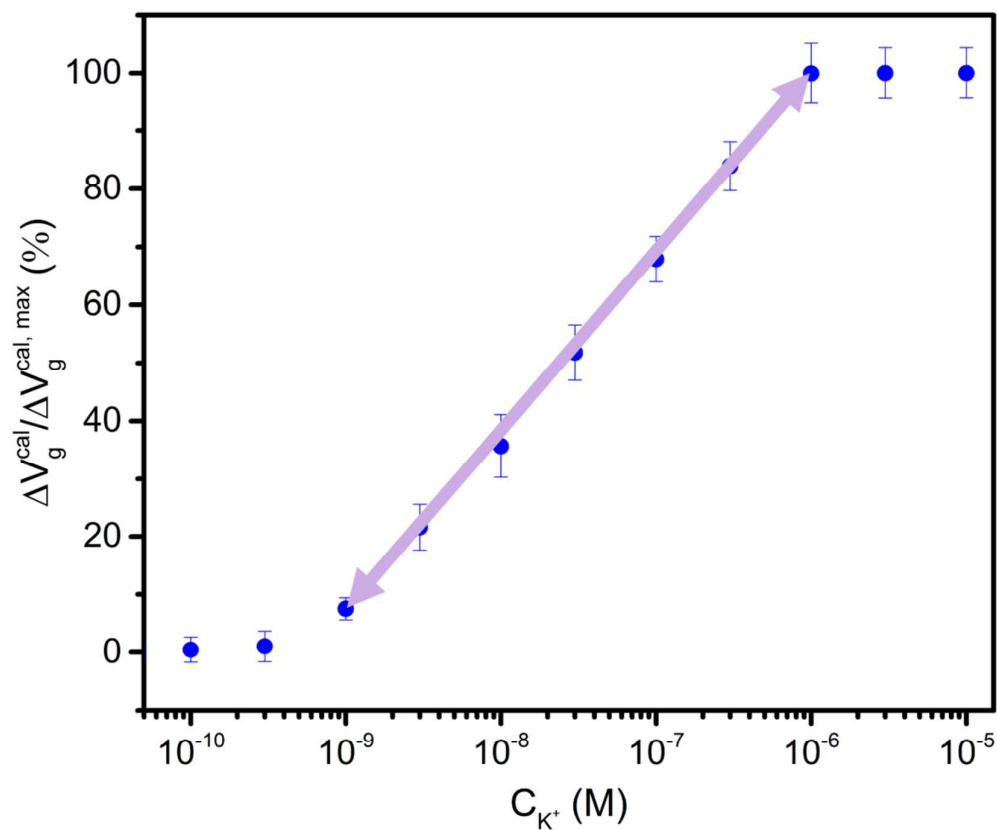
Figure S4. Comparative responses of a PTMS/SiNW-FET and an aptamer/SiNW-FET to different C_{K^+}. (a) The I_{sd}–V_g curves of a PTMS/SiNW-FET without the aptamer modification shows no significant response to different C_{K^+}. The magnified scale is shown in the inset. (b) The calibrated responses ($\Delta V_{g,K^+}^{cal}$) of an aptamer/SiNW-FET (red columns) or a PTMS/SiNW-FET (black columns) in response to different C_{K^+}. The data measured by aptamer/SiNW-FET (red columns) were taken from Figure 2a and presented as the mean ± the standard deviation from 3 independent measurements.
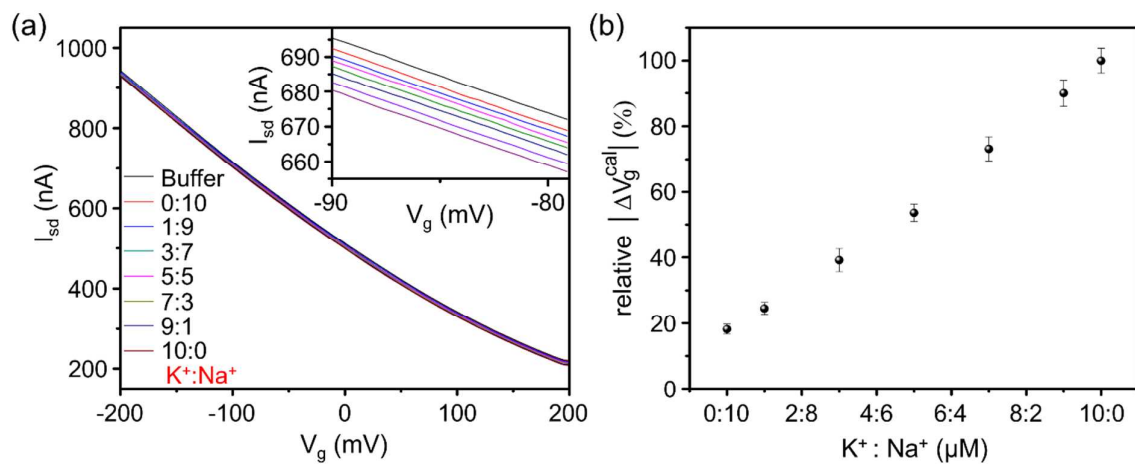
Figure S5. The target-selectivity of an aptamer/SiNW-FET was tested against various biologically relevant ions, including K^+, Ca^{2+}, Li^+, and Cs^+.

Figure S6. A semi-log plot of $\Delta V_g^{cal}/\Delta V_g^{cal,max}$ as a function of C_{K^+}. The linear working range of this aptamer/SiNW-FET device spans from approximately 10^{-9} to 10^{-6} M as marked by the double arrows.

Figure S7. An aptamer/SiNW-FET senses K^+ ions in the presence of Na^+ ions. (a) The $I_{sd}-V_g$ curves of an aptamer/SiNW-FET were measured in a 10 μM mixture of Na^+ and K^+ ions with different ratios. (b) The measured $\Delta V_g^{cal}/\Delta V_g^{cal,max}$ as a function of different concentration ratios of K^+: Na^+. The ΔV_g^{cal} data were taken from (a) at V_g = -90 mV. The data presented were the mean ± the standard deviation from 3 independent experiments.

References

[S1] Li, B.-R.; Hsieh, Y.-J.; Chen, Y.-X.; Chung, Y.-T.; Pan, C.-Y.; Chen, Y.-T. An Ultrasensitive Nanowire-Transistor Biosensor for Detecting Dopamine Release from Living PC12 Cells under Hypoxic Stimulation. *J. Am. Chem. Soc.* **2013**, *135*, 16034–16037.

[S2] Guo, Y.; Chen, Y.; Wei, Y.; Li, H.; Dong, C. Label-Free Fluorescent Aptasensor for Potassium Ion Using Structure-Switching Aptamers and Berberine. *Spectrochim. Acta Mol. Biomol. Spectrosc.* **2015**, *136*, 1635–1641.

[S3] Yuanboonlim,W.; Siripornnoppakhun, W.; Niamnont, N.; Rashatasakhon, P.; Vilaivan, T.; Sukwattanasinitt, M. Phenylene–Ethynylene Trication As an Efficient Fluorescent Signal Transducer in an Aptasensor for Potassium Ion. *Biosens. Bioelectron.* **2012**, *33*, 17–22.

[S4] Liu, Y.Y.; Li, B. X.; Cheng, D. M.; Duan, X. Y. Simple and Sensitive Fluorescence Sensor for Detection of Potassium Ion in the Presence of High Concentration of Sodium Ion Using Berberine–G-Quadruplex Complex As Sensing Element. *Microchem. J.* **2011**, *99*, 503–507.

[S5] Fan, X. Y.; Li, H. T.; Zhao, J.; Lin, F. B.; Zhang, L. L.; Zhang, Y. Y. A Novel Label-Free Fluorescent Sensor for the Detection of Potassium Ion Based on DNAzyme. *Talanta* **2012**, *89*, 57–62.

[S6] Shi, C.; Gu, H. X.; Ma, C. P. An Aptamer-Based Fluorescent Biosensor for Potassium Ion Detection Using a Pyrene-Labeled Molecular Beacon. *Anal. Biochem.* **2010**, *400*, 99–102.

[S7] Sun, H.; Li, X.; Li, Y.; Fan, L.; Kraatz, H. B. A Novel Colorimetric Potassium Sensor Based On the Substitution of Lead from G-Quadruplex. *Analyst* **2013**, *138*, 856–862.

[S8] Chen, Z.; Huang, Y.; Li, X.; Zhou, T.; Ma, H.; Qiang, H.; Liu, Y. Colorimetric Detection of Potassium Ions Using Aptamer-Functionalized Gold Nanoparticles. *Analytica Chimica Acta.* **2013**, *787*, 189–192.

[S9] Chen, Z.; Guo, J.; Zhang, S.; Chen, L. A One-Step Electrochemical Sensor for Rapid Detection of Potassium Ion Based on Structure-Switching Aptamer. *Sens. Actuator B-Chem.* **2013**, *188*, 1155–1157.

[S10] Jarczewska, M.; Górski, L.; Malinowska, E. Application of DNA Aptamers As Sensing Layers for Electrochemical Detection of Potassium Ions. *Sens. Actuator B-Chem.* **2016**, *226*, 37–43.

[S11] Miao, P.; Tang, Y.; Wang, B.; Han, K.; Chen, X.; Sun, H. An Aptasensor for Detection of Potassium Ions Based on Recj(F) Exonuclease Mediated Signal Amplification. *Analyst* **2014**, *139*, 5695–5699.

[S12] Wang, G.; Chen, L.; Zhu, Y.; He, X; Xu, G.; Zhang, X. Development of an Electrochemical Sensor Based on the Catalysis of Ferrocene Actuated Hemin/G-Quadruplex Enzyme for the Detection of Potassium Ions. *Biosens. Bioelectron.* **2014**, *61*, 410–416.